Published in final edited form as:
Neuroscience. 2006 November 3; 142(4): 1093–1117.

ABUNDANCE AND ULTRASTRUCTURAL DIVERSITY OF NEURONAL GAP JUNCTIONS IN THE OFF AND ON SUBLAMINAE OF THE INNER PLEXIFORM LAYER OF RAT AND MOUSE RETINA

N. KAMASAWA[a], **C. S. FURMAN**[b], **K. G. V. DAVIDSON**[a], **J. A. SAMPSON**[a], **A. R. MAGNIE**[a], **B. R. GEBHARDT**[a], **M. KAMASAWA**[a], **T. YASUMURA**[a], **J. R. ZUMBRUNNEN**[c], **G. E. PICKARD**[a,d], **J. I. NAGY**[e], and **J. E. RASH**[a,d,*]

a *Department of Biomedical Sciences, Colorado State University, Campus Delivery 1617, Fort Collins, CO 80523, USA*

b *Department of Physiology, Southern Illinois University School of Medicine, Southern Illinois University at Carbondale, Carbondale, IL 62901, USA*

c *Department of Statistics, Colorado State University, Fort Collins, CO 80523, USA*

d *Program in Molecular, Cellular and Integrative Neurosciences, Colorado State University, Fort Collins, CO 80523, USA*

e *Department of Physiology, Faculty of Medicine, University of Manitoba, Winnipeg, Manitoba, Canada R3E 3J7*

Abstract

Neuronal gap junctions are abundant in both outer and inner plexiform layers of the mammalian retina. In the inner plexiform layer (IPL), ultrastructurally-identified gap junctions were reported primarily in the functionally-defined and anatomically-distinct ON sublamina, with few reported in the OFF sublamina. We used freeze-fracture replica immunogold labeling and confocal microscopy to quantitatively analyze the morphologies and distributions of neuronal gap junctions in the IPL of adult rat and mouse retina. Under “baseline” conditions (photopic illumination/general anesthesia), 649 neuronal gap junctions immunogold-labeled for connexin36 were identified in rat IPL, of which 375 were photomapped to OFF vs. ON sublaminae. In contrast to previous reports, the volume-density of gap junctions was equally abundant in both sublaminae. Five distinctive morphologies of gap junctions were identified: conventional crystalline and non-crystalline “plaques” (71% and 3%), plus unusual “string” (14%), “ribbon” (7%) and “reticular” (2%) forms. Plaque and reticular gap junctions were distributed throughout the IPL. However, string and ribbon gap junctions were restricted to the OFF sublamina, where they represented 48% of gap junctions in that layer. In string and ribbon junctions, curvilinear strands of connexons were dispersed over 5 to 20 times the area of conventional plaques having equal numbers of connexons. To define morphologies of gap junctions under different light-adaptation conditions, we examined an additional 1150 gap junctions from rats and mice prepared after 30 min of photopic, mesopic and scotopic illumination, with and without general anesthesia. Under these conditions, string and ribbon gap junctions remained abundant in the OFF sublamina and absent in the ON sublamina. Abundant gap junctions in the OFF sublamina of these two rodents with rod-dominant retinas revealed previously-undescribed but extensive pathways for inter-neuronal communication; and the wide dispersion of connexons in string and

*Correspondence to: J. E. Rash, Department of Biomedical Sciences, Colorado State University, Campus Delivery 1617, Fort Collins, CO 80523, USA. Tel: +1-970-491-5606; fax: +1-970-491-7907. E-mail address: john.rash@colostate.edu (J. E. Rash)..

Available online 28 September 2006

ribbon gap junctions suggests unique structural features of gap junctional coupling in the OFF vs. ON sublamina.

Keywords

connexin36; Cx36; freeze-fracture replica immunogold labeling; FRIL; confocal immunocytochemistry

---

In the mammalian retina, vertical neuronal communication from photoreceptor cells, ultimately to output ganglion cells, is propagated primarily by conventional chemical synapses. In addition, gap junctions/electrical synapses also contribute to both lateral and vertical communication pathways (Cook and Becker, 1995; Vaney, 2002; Wässle, 2004; Sterling and Demb, 2004). In mammals, gap junctions are composed of "connexin" proteins that range from 25 kDa (Cx25) to 62 kDa. Connexin molecules assemble as hexameric transmembrane tubes ("connexons") that link head-to-head across the extracellular space to form intercellular channels for direct exchange of ions and small molecules (Bennett, 1997). In retinal neurons, at least three connexins—connexin36 (Cx36), connexin45 (Cx45) and connexin57 (Cx57)—are expressed (Condorelli et al., 1998; Güldenagel et al., 2000; Maxeiner et al., 2003, 2005; Hombach et al., 2004). Cx36 is, by far, the most abundant, both in outer plexiform layer (OPL) and inner plexiform layer (IPL). In contrast, Cx57 is present only in horizontal cell processes within the OPL (Hombach et al., 2004), and Cx45 is present in a small subset of neurons in both the IPL and OPL (Güldenagel et al., 2000; Han and Massey, 2005; Schubert et al., 2005b). Cx36 is essential in the rod-mediated vertical signaling pathway: in Cx36 knockout mice, all synaptic communication from rods to ON-center ganglion cells is eliminated (Deans et al., 2002). In that regard, Cx36-immunofluorescence is most abundant at narrow-field bi-stratified rod amacrine (i.e. AII amacrine), cone bipolar, and ganglion cells of the proximal IPL (i.e. physiologically-defined "ON" sublamina) (Feigenspan et al., 2001, 2004; Mills et al., 2001; Hidaka et al., 2002, 2004; Deans et al., 2002). Although a few Cx36-puncta were also detected in the distal IPL ("OFF" sublamina) in rats, mice and rabbits (Güldenagel et al., 2000; Feigenspan et al., 2001; Mills et al., 2001), quantitative data are not available for gap junctions nor are the cells linked by gap junctions identified in that sublamina.

Initially, "plaque" gap junctions with hexagonally-packed intramembrane particles (IMPs) were found in freeze-fracture replicas of the OPL in rabbit and monkey retinas (Raviola and Gilula, 1973, 1975). In addition, several examples of unusual linear arrays of connexon-like IMPs were identified as gap junctions in OPL of light-adapted monkey and rabbit retina, based on their uniform 9-nm diameter and regular 10-nm spacing (Raviola and Gilula, 1973). Similar linear gap junctions were also identified in OPL of human retina (Reale et al., 1978). However, in the mammalian *IPL*, only plaque gap junctions have been described. By thin-section transmission electron microscopy (TEM), close membrane appositions clearly identified as gap junctions were described in the ON sublamina, including between ON-cone bipolar cells, between AII amacrine cells, and between AII amacrine cells and ON-cone bipolar cells [(Kolb, 1979; Strettoi et al., 1992; Tsukamoto et al., 2001); reviewed by Sterling and Demb (2004)]. In the OFF sublamina, small gap junctions were also reported between OFF-cone bipolar cells (Kolb, 1979), but TEM images were not provided. Even with those studies, morphological classification and mapping of gap junctions in OFF vs. ON sublaminae in different species and/or under different physiological conditions have not been possible because insufficient numbers of neuronal gap junctions were detected to permit quantitative analysis and because different morphologies of gap junctions were not easily recognized in thin sections. Freeze-fracture replica immunogold labeling (FRIL), which provides for efficient detection and ultrastructural mapping of membrane proteins (Fujimoto, 1995; Rash and Yasumura, 1999), has facilitated detection, immunocytochemical identification, and mapping of Cx36 in

ultrastructurally-defined neuronal gap junctions in various regions of the mammalian CNS, including retina (Rash et al., 2000, 2001, 2004; Ciolofan et al., 2006).

In this study, FRIL was used to quantify and ultrastructurally categorize 931 neuronal gap junctions in the IPL of rat retina and to examine an additional 866 gap junctions in mouse IPL. For initial analysis, we obtained a statistically-robust population of neuronal gap junctions (649) in rat IPL fixed by vascular perfusion with formaldehyde under a single preparation protocol (photopic illumination and general anesthesia). From this "baseline" population, we identify five distinctive morphologies of gap junctions: crystalline plaques, non-crystalline plaques, plus string, ribbon, and reticular configurations. We show that these forms are differentially distributed within the IPL, with string and ribbon configurations restricted almost exclusively to the OFF sublamina. However, quantitative data from FRIL and from three-dimensional confocal immunofluorescence microscopy revealed that rat retinas have equal volume-densities of gap junctions in the OFF vs. ON sublaminae. To determine whether the newly-described string and ribbon configurations represent adaptation to prolonged photopic conditions or to general anesthesia, we also examined rat and mouse retinas adapted to scotopic and mesopic illumination, with and without anesthesia. Under all light-adaptation and anesthesia conditions investigated, string and ribbon gap junctions remained abundant in the OFF sublamina and did not appear in the ON sublaminae. The abundance of gap junctions in the OFF sublamina and the wide variety of morphologies and sizes of those gap junctions indicate the existence of previously unknown gap junction communication pathways in the OFF sublamina of these animals with rod-dominant retinas.

EXPERIMENTAL PROCEDURES

All animals used in this study were prepared under protocols approved by the Institutional Animal Care and Use Committees of Colorado State University and the University of Manitoba and conducted according to *Principles of Laboratory Animal Care* (U.S. National Institutes of Health Publication No. 86-23, Rev. 1985). These protocols included minimization of stress to animals and minimization of number of animals used.

Immunofluorescence microscopy

Four adult male Sprague–Dawley rats (300 g) were prepared for immunofluorescence analysis of Cx36 in retina, as previously described (Ciolofan et al., 2006). Rats were deeply anesthetized with equithesin and transcardially perfused with a series of three solutions consisting of 10 ml of cold pre-wash (50 mM sodium phosphate buffer, pH 7.4, 0.9% NaCl, 0.1 sodium nitrate and 1 unit/ml heparin), followed by 300 ml of cold fixative (0.16 M sodium phosphate buffer, pH 7.6, 1% formaldehyde, 0.2% picric acid), followed by 10 ml of post-wash (25 mM sodium phosphate buffer, pH 7.4, 10% sucrose). Immediately following perfusion fixation, the rats were decapitated, consistent with recommendations of the Capital Panel on Euthanasia of the American Veterinary Association. Eyes were removed, stored at 4 °C for 24–72 h in cryoprotectant consisting of the post-wash. Vertical sections of retina (10 μm thick) were cut on a cryostat and collected on gelatinized glass slides. Sections were washed for 20 min in 50 mM Tris–HCl buffer (pH 7.4) containing 0.256 M sodium chloride (TBS) plus 0.3% Triton X-100 (TBSTr), and incubated for 24 h at 4 °C with anti-Cx36 antibody Ab36–4600 (Invitrogen/Zymed Laboratories Inc., South San Francisco, CA, USA) at a concentration of 1 μg/ml in TBSTr containing 5% normal donkey serum. The specificity of affinity-purified anti-Cx36 Ab36–4600 has been demonstrated by showing absence of immunolabeling in retinas of Cx36 knockout mice (Li et al., 2004). Sections were washed in TBSTr for 1 h at room temperature, and incubated for 1.5 h at room temperature with Alexa Fluor 488-conjugated donkey anti-rabbit immunoglobulin G (IgG) (Molecular Probes, Eugene, OR, USA) diluted 1:1000 in TBSTr. After secondary antibody incubations, sections were washed in TBSTr for

20 min; then in 50 mM Tris–HCl buffer, pH 7.4, for 30 min; and coverslipped with antifade medium. Fluorescence was examined on an Olympus Fluoview IX70 confocal microscope with image capture using Olympus Fluoview software.

Images were assembled using Adobe Photoshop CS (Adobe Systems, San Jose, CA, USA). Contrast range was maximized using "levels." For detection of weakly fluorescent puncta and comparison to images prepared as above, some images were analyzed with the midrange of "levels" set very close to the "dark output" level. This manipulation was required due to large differences in immunofluorescence labeling intensities observed in the OFF vs. ON sublamina; low in the former, high in the latter. To adequately represent comparisons of these intensities, confocal scans were taken of the entire IPL (rather than by separate scans of the OFF and ON sublamina) using optimal laser power, photo-multiplier or gain settings for visualization of puncta in each sublamina. As required by most journals, any manipulations of levels were applied to full images, rather than portions thereof. Thus, immunofluorescence images are presented as two sets, with optimization of saturation settings for visualization of puncta in either the ON or OFF sublamina. For generation of stereoscopic confocal immunofluorescence images, a z-stack of 29 images taken at 0.37 um intervals was used to make a two-dimensional projection for the left image. For the right image, the original Z-stack was used to generate a second projection having a horizontal offset of 7° from that of the left Z-stack projection. The two images form a stereoscopic pair that may be viewed either with crossed eyes or using a parallel-axis stereopticon-type viewer.

FRIL

Rats prepared under "baseline" photopic conditions and general anesthesia— Seven adult Sprague–Dawley rats (five males, two females, 101–547 g) were maintained in a 12-h light/dark cycle. Six hours after light onset, they were exposed to continuous bright light (3000–6700 lux) for 30 min prior to anesthesia and throughout fixation, thereby approximating the photopic conditions and methods of anesthesia used in previous freeze-fracture studies of rabbit and monkey retina (Raviola and Gilula, 1973, 1975; Raviola and Raviola, 1982). High photopic conditions were obtained by using two 150 W reflector flood lamps at 18 inches or by using a Kodak Ektagraphic E2 35 mm slide projector, with 300 W halogen bulb, held at 3 feet and projected directly at the rat before and during perfusion fixation. Illumination at the head of the rat was measured using a Tektronix J1811 cosine-corrected illuminance head attached to a Tektronix J17 photometer/radiometer/colorimeter (Tektronix, Inc., Wilsonville, OR, USA). During light adaptation, rats were cooled by air from a fan blowing across ice suspended above the cage. The rats were deeply anesthetized for 3–5 min following i.p. injections of ketamine plus xylazine (120–160 mg/kg and 12–16 mg/kg, respectively) and fixed by whole body vascular perfusion with 1% or 2% formaldehyde in Sørensen's phosphate buffer (SPB, 1:5 mixture of 0.15 M NaH_2PO_4 and 0.15 M Na_2HPO_4; pH 7.4), plus 0.05% sodium azide. [Formaldehyde is used for chemical fixation (rather than glutaraldehyde) because glutaraldehyde, even at 0.001% for 5 min, cross-links proteins so completely that the tissues cannot be cleaned with sodium dodecylsulfate detergent (SDS) (Rash and Yasumura, 1999), which is a requirement for FRIL (Fujimoto, 1995). However, because formaldehyde is a weaker cross-linking agent, subsequent chilling of samples may produce temperature-dependent "phase separation" of lipids and resultant clumping of membrane proteins (Maul, 1979) that may superficially resemble gap junctions. Criteria for discriminating gap junctions from clumped IMPs are presented in the Results]. Unlike injection of fixative into the posterior chamber of the eye, perfusion fixation utilizes the short diffusion distances from capillaries that permeate the retina. After formaldehyde fixation, the eyes were removed, the vitreous body was injected with formaldehyde in SPB, and the eyes were stored for 24 h in fixative at 4 °C.

Comparison of rats and mice adapted to photopic, mesopic and scotopic illumination; with and without general anesthesia—An additional 4 rats and 11 mice (4 albino, 6 C57BL and 1 CL3) were exposed to photopic (see above), mesopic (i.e. 0.02–0.05 lux) and scotopic (i.e. 0 lux) illumination for >30 min prior to anesthesia or in the absence of general anesthesia (with euthanasia by cervical dislocation) (Table 1). For examination of retinas prepared under scotopic and mesopic conditions, animals were obtained 6 h after light offset. For perfusion under scotopic and mesopic conditions, animals were visualized using Model #NE 5001 UL night-vision goggles (ITT industries, Roanoke, VA, USA) and infrared illumination. C57BL and CL3 mice, whose retinas contain pigment granules in their retinal pigment epithelium, were also compared with both albino mice and albino rats, which lack the protective pigment granules. Additional general anesthetics included halothane (administered using a rodent non-rebreathing circuit with 1.5 L/min O_2 and 1.5–2% halothane) and pentobarbital (80 mg/kg). Six adult mice and two juvenile rats (<200 g) were killed by cervical dislocation (Table 1) under protocols approved and monitored by a licensed veterinarian.

Preparation of tissues for FRIL—Rat retinas were dissected and suspended in gelatin blocks, and cut into 100 μm- or 150 μm-thick vertical slices using a refrigerated Lancer Vibratome 3000 (Technical Products International, St. Louis, MO, USA) that maintained samples at 4 °C. Although rats are nocturnal animals with rod-dominated retinas consisting of 99% rods and 1% cones (LaVail, 1976), rod- and cone-bipolar cells, amacrine cells, and ganglion cells are present at densities comparable to those in other mammals, and most of these cell classes are relatively evenly distributed across the central 4 mm of retina, each varying by less than 50% in density within that large area (Euler and Wässle, 1995). Vertical slices of rat retina were dissected to ca. 4 mm length (thereby eliminating edges having significantly lower densities of bipolar cells), then infiltrated with 30% glycerol cryoprotectant to minimize ice crystal damage during freezing, mounted on aluminum "Slammer" supports (Heuser et al., 1981), and frozen by contact with a liquid nitrogen-cooled metal mirror (Ultra-Freeze MF7000, RMC Products, Tucson, AZ, USA). For *mouse* retinas, the entire retinal hemispheres were cut into 100 μm- or 150 μm-thick vertical slice and the central slices were mounted intact and frozen as above.

Frozen samples were fractured and replicated in a JEOL/RMC 9010C freeze-fracture device (JEOL, Tokyo, Japan), then bonded to gold "index" grids (Electron Microscopy Sciences, Fort Washington, PA, USA) using 1.5–2% Lexan (GE Plastics, Pittsfield, MA, USA) dissolved in ethylene dichloride, according to our detailed procedures (Rash et al., 1995, 2004; Rash and Yasumura, 1999). The Lexan-stabilized samples were thawed and photomapped with a Zeiss LSM510 Meta laser scanning confocal microscope, using either tissue autofluorescence or following staining with NeuroTrace Fluorescent Nissl Stains (Molecular Probes).

SDS washing: retention of proteins for immunogold labeling—In these formaldehyde-fixed samples, bulk tissue remnants were removed from the confocal-mapped replicas by washing with constant stirring for 29 h at 48.5 °C in 2.5% SDS detergent in 0.16% Tris–HCl buffer (pH 8.9). After the initial 4 h in the SDS solution, the samples were digested for 2–4 h in 2–4% collagenase D (Roche Applied Science, Indianapolis, IN, USA) in 0.15 M SPB, followed by an additional 18 h in SDS solution. As described in his original report (Fujimoto, 1995), SDS washing leaves a monolayer of macromolecules strongly adsorbed to the replica, as well as additional molecules that are strongly bound to those macromolecules that are directly adsorbed to the replica (Rash and Yasumura, 1999; Rash et al., 2004). It is these remaining transmembrane molecules and their strongly bonded accessory proteins that are labeled by FRIL (Li et al., 2004; Rash et al., 2004; Ciolofan et al., 2006).

Immunogold labeling—SDS-washed replicas were rinsed in blocking buffer (Dinchuk et al., 1987) consisting of 10% heat-inactivated goat serum plus 1.5% fish gelatin in SPB, pH

7.4, and labeled for 60–220 min using various combinations of monoclonal and polyclonal antibodies diluted to 10 μg/ml in blocking buffer. Antibodies to Cx36 included mouse monoclonal Ab51–6300 (Invitrogen/Zymed) and previously characterized rabbit polyclonal Ab298 (Rash et al., 2000) and rabbit polyclonal Ab36–4600 (Invitrogen/Zymed). Rabbit antibody to zonula occludens-1 (ZO-1) was Ab61–7300 (Invitrogen/Zymed). After primary labeling, samples were rinsed and counter-labeled for 16 h using goat anti-rabbit IgG and goat anti-mouse IgG, each conjugated with a separate size of uniform-diameter gold beads (6-nm, 12-nm or 18-nm; Jackson ImmunoResearch Laboratories, West Grove, PA, USA; or 10-nm and 20-nm from Chemicon International, Inc., Temecula, CA, USA; the latter discontinued in 2000). After immunogold labeling, each sample was air-dried and coated on the labeled side with 10–20 nm of evaporated carbon to anneal cracks in the replica, as well as to stabilize the immunogold beads. Before viewing by TEM, the Lexan support film was removed by immersing the grids in ethylene dichloride solvent for 2–3 h, and the samples were again air-dried.

Radius of immunogold labeling

In the double-antibody "sandwich" technique (Fig. 1A), the primary antibody (mouse or rabbit IgG) is first reacted with its antigen, and a second antibody (goat anti-mouse IgG or goat anti-rabbit IgG) with an attached gold bead is used to label the primary antibody. This produces a 26–30-nm double-antibody bridge (Fig. 1) between the connexon and the immunogold beads (Matsubara et al., 1996;Ottersen and Landsend, 1997;Nagy et al., 1999). When air dried, compressive forces of surface tension cause most gold beads to collapse radially onto the replica, all the while maintaining the ca. 28-nm separation from the 9-nm connexon (Fig. 1B). Thus, gold beads do not remain directly superimposed on the connexons that are labeled, often appearing up to 28 nm beyond the edge of plaques, and almost all occurring within 28 nm from connexon strings. In selected images, this "zone of immunogold labeling" for connexons in identified gap junctions is indicated by *yellow overlays.*

A second source of displacement of immunogold beads arises from the process of SDS washing. As documented in osmium-fixed and uranyl acetate/lead citrate-stained FRIL replicas (Rash and Yasumura, 1999), partially-solubilized vesicular membrane fragments of gap junctions are often immobilized while carrying a few connexin proteins into solution (diagram; Fig. 1C). Because FRIL labeling is based on incomplete washing so that some proteins remain for labeling, partially-dissolved blebs, with their attached labels, are an ever-present reminder of the necessarily incomplete washing process. Based on stereoscopic analysis of those osmium-stained replicas, ca. 5% of immunogold beads were 50–80 nm from the margins of gap junctions. In samples with low background, labeling was restricted almost exclusively to replicated gap junctions, with immediately adjacent clusters of gold considered to represent specific labeling of unstained membrane "blebs." Specificity of labeling is assumed when the target protein arrays (e.g. cell-type-specific gap junctions) are labeled at a density at least 1000× greater than for gap junctions in other cell types and 1000× greater than for any other identifiable structure or IMP array. With signal-to-noise ratios usually >10,000:1 (Meier et al., 2004), we had high confidence in specificity of labeling.

A third source of displaced gold labels occurs when primary or secondary antibodies aggregate to form small to large clumps containing a few to several thousand or more gold beads (Rash and Yasumura, 1999). Although clumping occurs to a variable extent with all primary and secondary antibodies, particularly after multiple freeze–thaw cycles (Rash and Yasumura, 1999), FRIL allows for early detection and assessment of the extent and nature of antibody clumping and early discarding of aging labeling reagents. Although similar clumping of labels undoubtedly occurs for reagents used in immunofluorescence imaging, small clumps that initially amplify signals (as documented by FRIL) may not be recognized as a developing

artifact until large puncta are seen in inappropriate locations (e.g. in areas presumed not to contain gap junctions).

Electron microscopy

Replicas were examined at 100 kV in JEOL 2000 EX-II and JEOL 1200 EX TEMs (JEOL USA, Inc., Peabody, MA, USA). At low magnification, the larger 12-nm and 18-nm gold beads were easily detected in the 10,000× image viewed using 10× binoculars. By constantly tilting and adjusting focus, gap junctions were found even in steeply-contoured areas of the replica. Gap junctions that had been detected based on presence of gold "flags" were photographed stereoscopically (8° included angle) at high magnification (typically, 30,000×–100,000×). For photomapping, low magnification TEM images (500× or 600×) were obtained for each gap junction. Stereoscopic images were used for assessing complex three-dimensional membrane topography, as well as for confirming that each immunogold bead was on the tissue-side of the replica (Rash and Yasumura, 1999) and for discriminating the smaller (6-nm) gold beads from the equally-electron-opaque granularity of the platinum replica (Pereda et al., 2003a; Rash et al., 2004). All negatives were digitized by an ArtixScan 2500f digital scanner (Microtek; Carson, CA, USA) and processed using Adobe Photoshop 7.01 and/or Photoshop CS, using minimal (or no) "unsharp mask," maximal contrast expansion with "levels," and selected area "dodging" using brightness/contrast functions to optimize image contrast and definition.

Determination of dispersion coefficient (D_C) of connexons in gap junctions

For each morphological type of gap junction, 10 to 20 representative images were enlarged to 100,000× or 150,000×. The smallest ellipse whose outline would enclose the entire gap junction was superimposed using Photoshop. The orientation of the major axis of the ellipse was adjusted to correspond to the maximum diameter of the gap junction, and both the major and minor orthogonal axes were adjusted to enclose all connexons within the gap junction. The enclosed area for each ellipse was measured using Scion Image Beta 4.02 Win (Scion Corporation, Frederick, MD, USA), and the numbers of connexons were counted manually. Because quantitative data could not be collected from areas in which the fracture plane exited a gap junction and entered cytoplasm or extracellular space, these areas were subtracted from each ellipse (i.e. the shaded portions in the micrographs that were used to calculate D_C). Frequently, the fracture plane stepped from the *e*xtraplasmic fracture face ("E-face"); to the *p*rotoplasmic fracture face ("P-face") within the same gap junction. The internationally-recognized freeze-fracture terminology of Branton (1966) is used throughout this report. For each gap junction, the numbers of connexon P-face particles and E-face pits were counted. Strongly tilted gap junctions, as determined by stereoscopic imaging, were excluded from this analysis because of image foreshortening, which artifactually increases apparent connexon density. The density of connexons in "crystalline" plaque gap junctions, where connexons were in regular, close-packed hexagonal array, was found to be greatest (12,000 connexons per μm^2), and this value served as the basis for all other comparisons.

To quantify morphological differences between gap junctions having different configurations of connexons, we defined a quantitative descriptor called D_C, which reflects the average packing density of connexons within the smallest ellipse that would encompass all connexons within a single gap junction or gap junction complex. Operationally, D_C is defined as the maximum packing density of connexons (12,000/μm^2, as found in crystalline plaque gap junctions) divided by the number of connexons per μm^2 that were counted within the smallest ellipse that included all connexons within the target gap junction:

$$D_c = \frac{12,\ 000\,\text{connexons} / \mu\text{m}^2}{\#\ \text{connexons} / \mu\text{m}^2}$$

D_C is especially useful because it allows comparison of the potential "area of influence" of each gap junction (i.e. "pinpoint" vs. "diffuse" influence). For example, a value of $D_C = 20$ for a string gap junction signifies that the connexon components within the gap junction were dispersed over an area 20× larger than a crystalline plaque gap junction having the same number of connexons.

Data entry and compilation using Excel

Each immunolabeled gap junction was assigned an identification number and its grid map location was plotted on the corresponding low-magnification TEM and high-magnification light microscopy (LM) images. Connexons and immunogold beads of each size were counted manually. The number of connexons, number and sizes of immunogold beads on each gap junction, antibody species, source, and catalog number for each primary and secondary immunogold label, and other pertinent data were entered in Microsoft Excel X for correlation and statistical analysis.

Statistical analysis

For the baseline experiment, each type of gap junction (plaque, string, ribbon, and reticular), the proportion was compared in male vs. female rats. The analysis of variance tests were done with Proc Glimmix in SAS (SAS Institute, Inc., Release 9.1.3, Cary, NC, USA) with a logit transformation, a random rat within sex effect, and a fixed sex effect. None of the sex comparisons was significantly different ($P > 0.05$); consequently, sex as a category was omitted from subsequent models.

RESULTS

Criteria for FRIL mapping of neuronal gap junctions in retina

After freeze-fracturing but before SDS-washing and immunogold labeling, each replicated tissue slice was thawed and photographed on its gold "index" grid using laser scanning confocal microscopy (LM, Fig. 2A). These confocal images of Lexan-stabilized replicas were used to determine the orientation of the retina slice and to accurately map each gap junction found by FRIL. At low magnification, rat retinas appeared as concave bands, often extending completely across each 3-mm TEM grid, whereas the ca. 250-μm thickness of the retina extended across two or three grid openings (Fig. 2A, boxed area B). Each FRIL replica of the retina was compared with companion LM images fluorescently labeled for Cx36 (Fig. 2B). Between photoreceptor nuclei of the outer nuclear layer (ONL) and the interneurons of the inner nuclear layer (INL) was a thin layer (3–10 μm) of fluorescently-labeled neuropil constituting the OPL (Fig. 2B, C). Proximal to the INL was the IPL (Fig. 2B, D), a 30- to 50-μm thick layer of Cx36-immunolabeled neuropil, where complex synaptic pathways ultimately converge on ganglion cell dendrites. The proximal margin of the IPL was formed by the ganglion cell layer (GCL; Fig. 2B, D). Additional components of the retina, such as the outer and inner limiting membranes, retinal pigment epithelium (Fig. 2B), and the non-cellular vitreous humor, were also used as landmarks (not separately illustrated in FRIL images).

By FRIL, the very thin OPL (green overlay, Fig. 2C) was identified between the broad bands of nuclei comprising the ONL and INL (orange overlays). The much thicker IPL (Fig. 2D, green overlay) usually maintained continuity over large areas, allowing gap junctions to be mapped with respect to distances to both INL and GCL, thereby facilitating assignment of gap junctions to either OFF (distal 2/5) or ON sublaminae (proximal 3/5) (Euler and Wässle, 1995). When replicas of IPL were significantly wider than in true vertical section or did not include margins of both INL and GCL in the same or adjacent grid openings, none of the gap junctions in that grid opening were mapped to either OFF or ON sublaminae. Because the margin between the IPL and the GCL was undulated and irregular, reflecting the incursions of

ganglion cell somata into the lower IPL, we defined the local IPL/GCL margin as the point of deepest continuous incursion of neuropil into the GCL (Fig. 2D).

FRIL characterization of gap junctions in adult rat IPL under photopic ("baseline") conditions

The high visibility of larger gold beads (12-nm and 18-nm), relatively high labeling efficiency [LE≥1:10; LE defined as number of gold beads per number of connexons (Rash and Yasumura, 1999)], and a systematic search strategy allowed detection of 649 Cx36-containing gap junctions in the IPL from adult rats that had been anesthetized and fixed with formaldehyde under high photopic conditions. This large number permitted detailed quantitative and statistical analysis of the several gap junction morphologies and their sublaminar distributions. In 9 of 18 replicas, 375 labeled gap junctions were mapped to precise depths within the IPL; the remaining 274 gap junctions (mostly in the other 9 replicas) could not be accurately mapped, either because of local replica damage (e.g. cracks, tears and folds), one or both IPL margins were behind grid bars, or other technical problems. (Gap junctions and connexins in the OPL will be described in subsequent reports; Nagy et al., unpublished observations.) In IPL gap junctions, connexons were present in five distinctive configurations: 1) "crystalline plaques," 2) "non-crystalline plaques," 3) net-like or "reticular" arrays having large connexon-free voids, 4) double-strand or triple-strand "ribbons," and 5) single-strand "string" arrays.

Crystalline vs. non-crystalline "plaques"

Most commonly (74% of total number of gap junctions, 479/649), connexons were present in conventional "plaques" (Fig. 3), discrete aggregates of 9-nm P-face IMPs (connexons) or 6- to 8-nm E-face pits (connexon imprints) having 10-nm center-to-center spacing. Plaque gap junctions usually had no internal voids or discontinuities larger than the space occupied by a single connexon. Where the fracture plane stepped from P- to E-face, the extracellular space was narrowed to ca. 3 nm, another hallmark defining the IMP arrays as gap junctions. Moreover, the edges of gap junction plaque P- and E-faces were almost always precisely aligned, and the orientation of connexon rows within crystalline plaques was maintained at the step from P- to E-face (Fig. 3A). Finally, these gap junctions were immunogold-labeled for Cx36 at moderate to high LE and high specificity. Plaque gap junctions included both crystalline (Fig. 3A, B) and non-crystalline configurations of connexons (Fig. 3C, D).

Crystalline plaques—Under "baseline" conditions, most of the plaque gap junctions contained connexins in crystalline array (96% or 458/479; see Table 2), either as tightly packed clusters of P-face IMPs or E-face pits, usually in distinctive hexagonal arrays (Fig. 3A, B). Some of these contained one or more domains of quasi-crystalline hexagonal arrays of connexons (Fig. 3B). At the intersections of crystalline domains, an area sufficient to accommodate one connexon IMP/pit (occasionally two or three) was often present within the otherwise crystalline packing. Because of "plastic distortion" (stretching and inelastic rebound) of freeze-fractured transmembrane proteins (Steere et al., 1980) but absence of distortion of the pits from which the particles were removed (Rash and Yasumura, 1992), the crystalline hexagonal pattern was unaltered in E-face images but was often slightly altered in P-face images of gap junctions (Fig. 3A, B). Regardless, in all crystalline plaque gap junctions, the center-to-center spacing of P-face IMPs did not vary more than ±2 nm (i.e. 8–12 nm) due to plastic deformation (Hirokawa and Heuser, 1982).

Non-crystalline plaques—Under the same tissue preparation conditions, ca. 4% of plaque gap junctions (21/479) consisted of non-crystalline configurations of connexons (Fig. 3C, D). Although connexons in non-crystalline plaques sometimes had small regions of partial connexon regularity, most regions had slightly larger center-to-center distances between IMPs/pits (up to 15 nm vs. 10 nm in crystalline plaques), no clear hexagonal arrangement over the majority of the junction, and numerous small voids where one or occasionally two connexons

appeared to be missing. Consequently, the connexons in these plaques were less densely packed than in crystalline plaques.

Greater LE of gap junction E-face pits than of their P-face IMPs—As in all previous FRIL studies (Fujimoto, 1995; Rash and Yasumura, 1999; Rash et al., 2004), connexon E-face pits usually had noticeably higher labeling efficiencies than the adjacent P-face particles (Fig. 3A). This greater labeling of E-face pits vs. P-face particles was even more evident in other classes of gap junctions (see below). The increased LE of E-faces may be due to some protective factor of the replicated membrane E-face overlying the unfractured membrane beneath. In contrast, the removal of the protective external leaflet from P-face connexons and/or coating the exposed connexons with platinum/carbon apparently damages or alters them, making them substantially less likely to label than their unfractured neighbors beneath the adjacent E-faces.

"String" gap junctions

The second largest population (14%; 93/649) of Cx36-labeled gap junctions in rat IPL consisted of 1–30 curvilinear strands of connexons ("string" gap junctions; Fig. 4, red overlay), with most strands being one connexon wide and 0.1–0.7 μm long (or 10–70 P-face IMPs/E-face pits long). As in similar linear arrays in macaque and human *OPL* that were identified as gap junctions before the advent of immunogold labeling (Raviola and Gilula, 1973;Reale et al., 1978), these structures were identified as gap junctions based on the same criteria as plaque gap junctions: *a*) 9-nm P-face IMPs/8–9 nm E-face pits, *b*) uniform 10-nm center-to-center spacing of IMPs and pits, and *c*) where the fracture plane stepped from P-face to E-face, the extracellular space was narrowed to <3 nm (Fig. 4, black arrow). Moreover, similar linear gap junctions were first described in OPL in glutaraldehyde-fixed retina (Raviola and Gilula, 1973;Reale et al., 1978), demonstrating that string gap junctions are not artifacts of formaldehyde fixation. Free IMPs within the margins of string gap junctions, as well as nearby clusters of P-face IMPs (Fig. 4, *), were discounted as connexons because they were not of uniform 10-nm diameter (ranging from 6 to 12 nm), were variable in height and shape, and did not have uniform 10-nm center-to-center spacing.

Most string gap junctions had discontinuities in their rows of P-face IMPs and E-face pits, with their successive segments on either face almost always precisely aligned (Fig. 4A, white arrows), implying an underlying scaffolding structure that bridges the discontinuities. Although these linear arrays superficially resemble tight junctions, 100% of IMPs in string gap junctions are in the P-face and 100% of pits are in the E-face, whereas tight junctions in formaldehyde-fixed tissues have approximately 50% of the IMPs remaining with the E-face and 50% remaining with the P-face (Meier et al., 2004). In addition, tight junctions consist of continuous ridges and grooves (i.e. no separate IMPs or pits) on both fracture faces (Staehelin, 1974;Meier et al., 2004). Finally, these linear arrays were particularly well labeled for Cx36 [Fig. 4A; 6-nm gold beads (arrowheads) and 12-nm gold beads; Fig. 4B; 6-nm, 12-nm and 18-nm gold beads; overall LE of LE=1:3–1:10]. In contrast, tight junctions do not label for any connexin (Fujimoto, 1995). As in thin section immunogold labeling methods (Nagy et al., 1999), ca. 90–95% of immunogold beads were within 28 nm of the nearest connexons (Fig. 4B, yellow overlay), with gold beads rarely superimposed directly on individual connexon IMPs or pits (for explanation, see Fig. 1). The radial collapse of immunogold labels during air drying was particularly evident for string gap junctions (Fig. 4; diagrammed in Fig. 1B). [The five 18-nm gold beads in Fig. 4A represent labeling for ZO-1 (Li et al., 2004;Rash et al., 2004); see figure legend.]

"Ribbon" gap junctions

Under baseline conditions, 7% of Cx36-labeled gap junctions in IPL (47/649) had "ribbon" configurations of their constituent connexons (Fig. 5). (Despite similarity in names, ribbon gap

junctions should not be confused with “ribbon synapses” (Dowling and Boycott, 1966;Dowling, 1987), which contain a fence-like cytoplasmic density in nerve terminals of photoreceptor cells and bipolar cells (see Fig. 8A–B).) Connexon ribbons were similar to connexon strings, but in ribbons, each strand was predominantly either 2 or 3 connexons wide and up to 100 connexons long (Fig. 5A), often with short segments corresponding to string and/or plaque configurations (Fig. 5C–E). Connexons in ribbon gap junctions were especially well labeled for Cx36 (LE=1:5). As in other gap junctions, the extracellular space was narrowed at the step from P- to E-face (Fig. 5A, E; black arrows). Occasionally, gold beads were 50 – 80 nm from the margins of gap junctions (Fig. 5A, top of image), presumably corresponding to labeled membrane “blebs” stabilized by drying after the incomplete SDS washing required for FRIL (Experimental Procedures, Fig. 1C).

Distinguishing features of string and ribbon gap junctions

Intercellular structural coupling of connexons—As noted above for plaque gap junctions, the equal or greater efficiency of labeling of E-face pits in string and ribbon gap junctions, where the upper partner of each connexon pair had been removed, suggests that most if not all connexon E-face *imprints* retained their unreplicated connexon coupling partners in the underlying cell. Moreover, IMPs and pits of string and ribbon gap junctions were always precisely aligned at the step from E- to P-face. These two observations suggest that the connexons extracted from E-face pits had been structurally coupled to equal numbers of underlying connexon partners, thereby providing strong evidence for the presence of intact channels structurally linking the two cells, and against structural uncoupling to form linear arrays of unpaired hemichannels.

Polymorphic assembly—Most individual string and ribbon gap junctions contained predominantly either ribbon or string configurations (Fig. 5C vs. Fig. 5D), and each was defined based on its most abundant component. Nevertheless, many string and ribbon gap junctions were polymorphic, i.e. they contained multiple morphologies within a discrete connexon array (Fig. 5C–E). On rare occasions, string, ribbon and plaque configurations occurred together in virtually identical amounts within individual gap junctions (eight of 649; or ca. 1.2%), precluding their designation as either ribbon or string gap junctions (Fig. 5E). Thus, where appropriate, these polymorphic gap junctions are collectively included in a superclass of “linear” gap junctions (i.e. strings plus ribbons).

“Reticular” gap junctions

Gap junctions having one to six large connexon-free voids were also found (Fig. 6; 13/649 or 2.0% of total). When multiple voids were present, the perimeters of the junctions frequently were deeply indented. In these net-like or “reticular” gap junctions (previously called “anastomosing” gap junctions; Rash et al., 1997), the connexon-free voids were sufficiently large to contain 10–100 additional connexons (Fig. 6C vs. 6A). The voids within reticular gap junctions usually contained a few large *E-face* IMPs of unidentified composition (Fig. 6B, arrow). The inverse fracture pattern of these E-face IMPs clearly distinguished them from connexons, which in mammals are always in the P-face. Connexons surrounding the voids formed “septa,” which, unlike those in ribbons or strings, varied continuously in width, smoothly changing from 1 or 2 connexons wide, up to 10 connexons wide, and then back to 1 or 2 connexons. In the smallest reticular gap junctions, the septa formed distinctive shapes similar to the numerals “8” (Fig. 6B) and “0” (Fig. 6D). Although reticular gap junctions were relatively less common, this category was also seen in both OFF and ON sublaminae in mouse retinas prepared with and without general anesthesia (Fig. 6D).

Rare configurations: meandering, fragmented and complex arrays

In addition to the five distinctive configurations described above, other configurations of connexons were observed, but these were considered too rare (total <1.5%) to represent separate classes (images not shown). These included "meandering" arrays (*n*=2; 0.3% of total); "complex" gap junctions (*n*=5; 0.8%), which had separate domains corresponding to ribbon, string, and plaque portions; and "fragmented" gap junctions, which consisted of multiple small clusters of connexons that could not be assigned to plaque, ribbon, string, or reticular categories (*n*=2; or 0.3% of total).

Distribution of gap junction types in OFF vs. ON sublaminae

Based on photomapping (Fig. 2D; numbered triangles and circles), the five morphological types of gap junctions had distinctly different anatomical/sublaminar distributions (histogram, Fig. 7; also see Table 2). Plaque gap junctions were present in both sublaminae of the IPL (light gray bars in Fig. 7), but large plaque gap junctions (>400 connexons) were almost exclusively in the ON sublamina (39/40 large plaques). Reticular gap junctions were less abundant, but occurred in both sublaminae (horizontal cross-hatch in Fig. 7). In contrast, among 58 string gap junctions that were photomapped (black bars), 55 (95%) were localized to the OFF sublamina, and to the limit of our ability to map, the other 3 (5%) were in the outer part of the ON sublamina. Of those string gap junctions in the OFF sublamina, 60% were located within the outer half of the sublamina (approximately equivalent to stratum "1"; Euler and Wässle, 1995), and 40% were in the inner half (stratum "2"). The largest multi-stranded string gap junctions were found in stratum 2 of the OFF sublamina of IPL, near the border with the ON sublamina. In contrast, small string gap junctions were relatively evenly dispersed over the entire OFF sublamina. Likewise, ribbon gap junctions were restricted almost exclusively to the OFF sublamina (82%, or 14/17; bars with diagonal lines), and the remaining three were within the outermost portion of the ON sublamina (i.e. stratum 3 of IPL, near the border with the OFF sublamina), again demonstrating skewed sublaminar distributions of a second class of gap junctions having linearly dispersed connexons. In addition, five gap junctions (1.3%) resembling intermediate stages between strings and ribbons were found only in the OFF sublamina (diagonal cross-hatch). Overall, gap junctions consisting of linear arrays of connexons represented 48% (74/153) of all mapped gap junctions in the OFF sublamina. Because the vast majority of string and ribbon gap junctions were in the OFF sublamina, these two morphologies of gap junctions provided the most definitive gap junction markers for identifying the OFF sublamina in rat retinas prepared under photopic illumination (i.e. baseline conditions).

Statistical analysis of sublaminar distribution of gap junction types

Based on a large sample size of immunogold-labeled gap junctions, the relative proportions of plaque, ribbon, string and reticular gap junctions were compared between two locations (ON vs. OFF sublaminae; see Fig. 7 and Table 2). With a logit transformation, the analysis of variance model fit with Proc Glimmix included random effects for rat and for replica within rat, as well as analysis of fixed effects for type of gap junction, location, and type of gap junction by location. The type of gap junction by location interaction was statistically significant ($P<0.001$), which was due to the higher proportion of string and ribbon gap junctions in the OFF sublamina as compared with plaque gap junctions in both sublaminae.

Mixed synapses in both OFF and ON sublaminae of the IPL

In retina, "mixed" synapses (chemical plus electrical synapses; Sotelo and Korn, 1978) were first reported unmapped in human IPL (Reale et al., 1978), and later mapped to the ON sublamina of cat IPL (Kolb, 1979). By FRIL, mixed synapses were present in both OFF and ON sublaminae of the IPL. In the ON sublamina, plaque gap junctions labeled for Cx36 (Fig.

8A–B) were found at large terminals filled with synaptic vesicles, some of which were immediately adjacent to pre-synaptic ribbons (Fig. 8A–B, red arrowheads), thereby identifying these as axon terminals of either rod-bipolar or cone-bipolar cells. Because rod bipolar cells are reported not to have gap junctions (Kolb, 1979) or to express Cx36 (Feigenspan et al., 2004), the larger synaptic expansion at these mixed synapses were thus identified as ON-cone bipolar cells.

In the OFF sublamina, string gap junctions were also observed immediately adjacent to linear post-synaptic densities (PSDs) (Fig. 8C) characteristic of ribbon synapses (Raviola and Gilula, 1975;Reale et al., 1978;Raviola and Raviola, 1982). Because the only cells with large terminals and ribbon synapses in the OFF sublamina are OFF-cone bipolar cells, the presynaptic chemical component of this mixed synapse is identified as an OFF-cone bipolar cell. However, the post-synaptic component is not positively identified.

In addition to classically-defined mixed synapses, we also observed configurations consistent with the existence of "functionally-mixed synapses" (Pereda et al., 2003a,b, 2004). These were defined based on: 1) the presence of gap junctions, plus 2) densely-packed synaptic vesicles in either or both contacting neuronal processes, but 3) active zones or PSDs located several micrometers away from the gap junctions, or where the distance to the PSD or active zone could not be determined (Figs. 3A and 8D). One large crystalline plaque gap junction, consisting of >900 connexons, was found in the ON sublamina, linking one unidentified neurite to another neurite that contained abundant uniform-diameter synaptic vesicles (Fig. 3A). (Because FRIL frequently does not allow both apposed processes to be identified as either axon or dendrite, we use the term neurite only to designate that the unidentified process is of neuronal origin.) Large string gap junctions were also present on large chemical synaptic terminals in the OFF sublamina, some of which had abundant synaptic vesicles in both of the neurites that were linked by the gap junction strands (Fig. 8D). These synaptic expansions were consistent with either OFF-cone bipolar axon terminals or with "lobular dendrites" from AII amacrine cells. In either case, however, the relatively small sizes of these synapses (i.e. a few micrometers) as compared with the large "space constant" of neuronal cytoplasm in the retina [$\lambda = 200 – 410\ \mu$m; (Nelson, 1977)] implies that the gap junctions have the capability to affect both membrane potential and the dynamics of transmitter release at all locations within the synapse. Conversely, the functional state of gap junctions, if regulated by diffusion of chemical messengers, would be exquisitely sensitive to relative proximity of PSDs to the gap junctions (Pereda et al., 2004).

Single neurites may have multiple synaptic contacts, each with a separate gap junction

Multiple gap junctions were often shared by one neurite surface with two or three other nearby neurites (Fig. 9), and in all cases, their gap junctions were labeled for Cx36. This configuration demonstrates multiple electrical junctions between a single neurite and several other neurites, as originally shown in elegant serial thin-section reconstructions of ON-cone bipolar cell synapses in the ON sublamina (Kolb, 1979). FRIL revealed similar configurations in the OFF sublamina. In one case, three small string gap junctions labeled for Cx36 were observed on one neurite surface, each connected to an additional neurite (Fig. 9A). Thus, each connexon cluster was a separate gap junction linking different neurite pairs, rather than an isolated component of a single larger "composite" gap junction. Another synapse was linked by two ribbon gap junctions (Fig. 9B), where one small ribbon also extended into a plaque-like cluster of connexons. Where multiple gap junctions were observed between one neurite and one or more other neurites, almost all of their gap junctions (49/53) consisted of connexons in similar configurations (i.e. all strings, or all ribbons, or all plaques), suggesting coordinate regulation of the morphologies of all gap junctions locally linked to a single neurite.

Size variations of neuronal gap junctions

Neuronal gap junctions of all configurations varied enormously in their number of connexons (Fig. 10 and Table 2), from large (defined as >400 connexons); to "medium" (100–400 connexons), to small (2–100 connexons). Of the 479 plaque gap junctions found in IPL under "baseline" conditions, 15% (72/479) were large (Fig. 3A, B and Fig. 10A, B); 34% (164/479) were medium (Fig. 3D and Fig. 10C); and 51% (243/479) were small (Fig. 3C and Fig. 10D). The areas occupied by plaque gap junctions with regular margins (Fig. 10, white ellipses) precisely paralleled the number of connexons; however, not all plaque gap junctions had regular margins (Fig. 10B). The largest plaque gap junction found by FRIL in rat IPL under baseline conditions was 0.3 μm×0.5 μm and consisted of 1800 connexons (Fig. 10A). Under all light and anesthesia conditions investigated to date, the largest plaque gap junction of rat and mouse retina measured 0.4×0.5 μm and contained 2300 connexons (image not shown). In contrast, about half (51%) of plaque gap junctions were smaller than 0.1 μm in diameter (ca. 100 connexons), which is smaller than the limit of resolution of LM but potentially above the limit of immunofluorescence *detectability* (see Discussion). Moreover, ca. 25% of plaque gap junctions (120/479) were smaller than 50 connexons (Fig. 10D), demonstrating the existence of a large population of gap junctions consisting of very few connexons.

String and ribbon gap junctions also ranged from large (>400 connexons) to very small (<50 connexons). Large string (Fig. 4A) and large ribbon junctions (Fig. 5A) were rare (2.0% of string and ribbon gap junctions). Medium string gap junctions (100–400 connexons; Fig. 4B and Fig. 10E) constituted 30%, and small strings (Figs. 10F, G) represented 68%. Overall, string and ribbon gap junctions ranged from 0.1 μm to 2 μm in their longest dimensions.

In the photomapped gap junctions of all types (total 375), the OFF and ON sublamina had distinctly different size distributions of gap junctions and different total numbers of connexons (Table 2). In the OFF sublamina, 24% (36/153) of gap junctions were larger than 100 connexons, whereas 76% were smaller than 100 connexons. Moreover, ca. 35% were smaller than 50 connexons. In contrast, the ON sublamina had about half of its gap junctions larger than 100 connexons (53%; 118/222), and about half (47%) were smaller than 100 connexons, with ca. 25% smaller than 50 connexons. Overall, there were 12,700 connexons (in 153 gap junctions) in the OFF sublamina vs. 44,300 connexons (in 222 gap junctions) in the ON sublamina. When corrected for relative area examined, this means that despite the equal volume density of gap junctions, there were 2.3 times as many connexons per unit volume in ON vs. OFF sublamina.

D_C of neuronal gap junctions in IPL

Comparison of crystalline and non-crystalline plaques, reticular, string, and ribbon gap junctions revealed statistically-significant differences in D_C of their constituent connexons (Fig. 11). The tightly-packed connexons in *crystalline plaques* having smooth margins and consisting of a single domain in regular hexagonal array had the maximum connexon packing density of 12,000/μm^2 and the minimum D_C of unity (D_C=1.0, Fig. 10A, C, D, also see Fig. 3A–B), against which the relative dispersions of connexons in all other classes of gap junctions were compared. Because crystalline plaque gap junctions varied in shape from circles, ellipses and triangles, to relatively rare shapes with deeply indented outlines (Fig. 10B), the D_C for *irregularly-shaped crystalline plaques* were approximately twofold higher (D_C=2.1). In *non-crystalline plaques* (Fig. 3C, D), irregular spacing among connexons resulted in packing densities of 8000–11,000 connexons/μm^2, which combined with irregular outlines, yielded slightly larger D_C (D_C=1.3–2.7). *Reticular gap junctions*, even those with tightly packed connexons in their septa (Fig. 6) required disproportionately larger ellipses to enclose all of their connexons, resulting in D_C of D_C=2.0–7.4. *Ribbon gap junctions* (Fig. 5A) had large voids within their borders, thereby giving them still higher D_C (D_C=4.3–14.4). *String gap*

junctions were most dispersed (Fig. 10E–G, also see Figs. 4, 9), yielding D_C=4.8 to D_C=21. Graphic comparison of D_C for all classes of gap junctions is shown in Fig. 11A. If connexons are equally functional in all five classes of gap junctions (not established), the large differences in D_C may imply large differences in areas of chemical or metabolic influence.

Statistical analysis of D_C

The D_C as measured above were lognormal. Using the $\log_2$ transformation of D_C, the Proc Mixed procedure fit an analysis of variance model (Fig. 11B) that included random effects for rat and for replica within each rat, and a fixed effect for type of gap junction (crystalline plaque, non-crystalline plaque, ribbon, string, and reticular). The type of gap junction was a statistically significant effect (P<0.001). The crystalline and non-crystalline plaque means were not significantly different (P>0.05; Fig. 11B), and the ribbon and string means were not significantly different (P>0.05). However, both crystalline and non-crystalline plaque means were significantly smaller (P<0.01; *) than the reticular mean, and the reticular mean was significantly smaller (P<0.05; *) than both ribbon and string means.

Three-dimensional immunofluorescence microscopy

In stereoscopic projections (Fig. 12) of confocal stacks from a section of rat retina 10.6 μm thick and having an image width and height of 46.5 μm (i.e. 22,500 μm^3), 1049 Cx36-immunofluorescent puncta were counted. Of these, ca. 200 puncta were *not* detectable in glossy photographic prints (Fig. 12A) compared directly to images viewed by video monitor, a loss that is due to the more limited dynamic range of print media. Of the Cx36-immunofluorescent puncta, 1.5% (15 of 1049) were larger than 1 μm in diameter, and 11% (113/1049) were larger than 0.8 μm (Fig. 12A). In contrast, none (0%) of the plaque gap junctions seen by FRIL in a comparable sample size were larger than 0.4×0.5 μm. Thus, even the largest plaque gap junctions seen by FRIL in rat retina were much smaller than the large Cx36-immunofluorescent puncta.

In contrast to plaque gap junctions, the largest string gap junctions measured 2 μm×0.5 μm in FRIL images. Consequently, we considered whether these might correspond to the largest immunofluorescent puncta. However, 85% (96/113) of the large puncta were present only in the ON sublamina, where string gap junctions were not detected, demonstrating that large string gap junctions cannot correspond to the numerous large Cx36-immunofluorescent puncta seen in the ON sublamina. Therefore, in the ON sublamina of rats, most of the large immunofluorescent puncta (i.e. >0.8 μm) must arise from *plaque* gap junctions, almost all of which are smaller than 0.3 μm in diameter and contain <1000 connexons. This implies that pixel saturation and “halation” (apparent photon spread) occur even for medium-diameter plaque gap junctions. Likewise, in the OFF sublamina, 15% are large intensely fluorescent puncta, whereas *large* string gap junctions represent <2% of gap junctions. Thus, the few large string gap junctions cannot correspond to the numerous large puncta in either sublamina.

In stereoscopic images with contrast and brightness increased in the “dark output” range, diffuse puncta became more distinct, virtually filling stratum 2 and the border of stratum 3 (Fig. 12B, circles). These newly-revealed puncta presumably correspond to small gap junctions (50–100 connexons) *or* to those having diffuse Cx36 labeling, such as would occur in string gap junctions. In that regard, it is noteworthy that in the same image with increased brightness and contrast in the dark output range, resulting in gross oversaturation of large puncta, far fewer additional small puncta appeared in the ON sublamina (square boxes in stratum 4, Fig. 12A. vs. 12B), where string and ribbon gap junctions are rare or non-existent. This is consistent with the conclusion that small/diffuse puncta in the OFF sublamina represent an additional population of gap junctions that were necessarily not recognized previously because they were below fluorescence detectability when image saturation levels were set to optimize pixel

saturation levels in the ON sublamina. In any case, the entire OFF sublamina is now shown to contain abundant but weakly Cx36-immunofluorescent puncta, supporting quantitative data from FRIL.

Estimation of the number of gap junctions in rat IPL by FRIL vs. immunofluorescence LM

Quantification by FRIL—In FRIL replicas from the central retina of rats, 10–20 gap junctions typically were observed beneath each linear 70 μm of IPL exposed in each grid opening, yielding an average of ca. 0.4 gap junctions per linear μm of replicated IPL (see photomap in Fig. 2D). Each vertical section of adult rat retina has an average length of 6 mm (Euler and Wässle, 1995). With a hypothetical optimum fracturing interval of 0.5 μm to maximize encountering gap junctions [based on 0.5 μm average diameter of neurite processes in IPL, as measured from published thin-section images of rabbit (Kolb, 1979) and from FRIL images of rat retina (this study)], there would be ca. 12,000 potential non-overlapping full-width fractures per retina in the first orthogonal plane, yielding an estimated 28 million neuronal gap junctions in that plane of fracture. However, with three orthogonal planes for freeze fracturing, each fracture through a mixture of approximately spherical and cylindrical synaptic contacts can expose, on average, only about 1/3 (or 1/π) of the surface of each vesicle or cylinder (maximum is one half of any spherical or cylindrical process). Cross-fractures through cytoplasm further decrease the surface area capable of revealing gap junctions. Thus, from FRIL data, we estimate that there are ca. *90 million* gap junctions per IPL per rat retina (i.e. π×28,000,000). However, we also note that large gap junctions (>0.5 μm; or larger than the theoretical fracturing interval) on larger terminals are likely over-sampled, whereas small gap junctions on the smallest processes (<0.2 μm) are likely under-sampled. Because of the low level of precision of these estimates, no attempt is made to correct for any of these sources of systematic error.

Of all gap junctions detected in the IPL by FRIL, ca. 40% (estimated 36 million) were in the OFF sublamina. Approximately 45% of these were string and ribbon gap junctions (corresponding to ca. 16 million), and ca. 45% were plaque gap junctions (or ca. 16 million). Of the 400,000–830,000 cone-bipolar cells in rat retina (Euler and Wässle, 1995), ca. 50% are ON-cone bipolar cells that are reported to pass through the OFF sublamina without making chemical synapses or recognizable electrical synapses (Kolb and Famiglietti, 1974; Kolb, 1979). The remaining half are OFF cone-bipolar cells (ca. 200,000–415,000) plus their coupling partners in the OFF pathway, which presumably share the calculated 36 million Cx36-containing gap junctions in the OFF sublamina. This yields an estimated 88–180 gap junctions in each cellular *OFF-cone pathway*. (This pathway includes all combinations of synapses involving OFF-cone bipolar cells and their associated amacrine and ganglion cell dendrites.)

Calculations from immunofluorescence images—With conventional confocal scans (Fig. 12A) and with images processed to maximize detection of the smallest/least intensely fluorescent puncta (Fig. 12B), and with images viewed stereoscopically to visually separate superimposed puncta, comparison LM images of Cx36 immunofluorescence in rat IPL revealed abundant puncta. Based on the area and an estimated average 40-μm thickness of the IPL, the confocal images yielded an estimated 67 million gap junctions per IPL, or ca. 26% lower than the estimates from FRIL. Moreover, ca. 60% of puncta were counted in the ON sublamina and 40% in the OFF sublamina (Fig. 12B). Because this is also the same relative ratio of the thicknesses of these two layers, both techniques suggest that gap junctions are at about the same volume density in both sublaminae.

Mills et al. (2001) estimated that in rabbit retina, there are ca. 100 Cx36-positive fluorescent puncta per AII amacrine cells, which they suggested to represent ca. 98% of all puncta in the ON sublamina. Of these 84% were AII-AII and 16% were AII-cone bipolar cells. With 36 –

54 million gap junctions in the ON sublamina (as calculated from LM and FRIL data), and based on the assumptions that rat also has 98% of Cx36-containing gap junctions on AII amacrine cells, and that there are 100,000–150,000 AII amacrine cells per rat retina (Euler and Wässle, 1995), we calculate that there are 254–540 gap junctions per AII amacrine cell. However, this two- to fivefold higher number of gap junctions per AII amacrine cell in rat retina may indicate either: *a*) rat AII amacrine cells may have two- to fivefold more gap junctions than rabbit AII amacrine cells, but with most of those <100 connexons, b) rats but not rabbits have a population of unidentified neurons that have small Cx36-containing gap junctions, or c) in rabbit, there is a population of Cx36-containing gap junctions that are too small to have been detected previously.

String gap junctions occur in OFF sublamina of rats and mice under all light adaptation conditions

To determine if string and ribbon gap junctions represent static, cell-type specific structures *or* dynamic structures that alter their connexon configurations according to light adaptation or to exposure to general anesthesia, rat and mouse retinas were obtained under scotopic, mesopic and photopic illumination under different conditions of anesthesia (i.e. ketamine/xylazine, halothane, and pentobarbital, and cervical dislocation without anesthesia; Table 1). These replicas revealed no large-scale changes in the number or distribution of string and ribbon gap junctions. Under all conditions examined, similar numbers and distributions of linear gap junctions occurred in the OFF sublamina (Fig. 13), but few or none were observed in the ON sublamina. For example, in rats under *scotopic* illumination, with euthanasia by cervical dislocation, string gap junctions were detected in the IPL only in the OFF sublamina (Fig. 13A, B). Likewise, in *mice* killed by cervical dislocation under photopic illumination, string gap junctions also were detected only in the OFF sublamina (Fig. 13C). Overall, the five configurations of gap junctions in both rats and mice were present in the same laminae and in the approximate same ratios under scotopic and mesopic adaptation, with and without anesthesia, as were observed under photopic adaptation.

DISCUSSION

FRIL immunocytochemistry allowed quantitative ultrastructural analysis of the sizes, morphological diversity, and sublaminar distributions of Cx36-containing gap junctions in the IPL of adult rat retina after adaptation to photopic, mesopic and scotopic illumination. Based on our examination of more than five times the total number of retinal gap junctions in rat and mouse than in all other ultrastructural studies of mammalian retina combined, we defined five distinct arrangements of connexons within gap junctions of the IPL, where previously only plaque gap junctions had been described. While it had been suggested that gap junctions occurred primarily in the ON sublamina, we detected abundant Cx36-immunogold labeled gap junctions and corresponding immunofluorescent puncta throughout the IPL, demonstrating equal volume-density of gap junctions in both OFF and ON sublaminae. However, many of the gap junctions were much larger in the ON sublamina, thereby producing the 2.3-fold higher volume-density of *connexons* and overall greater immunofluorescence of that sublamina. Under initial “baseline” conditions (i.e. rats adapted to photopic illumination and fixed under general anesthesia), plaque gap junctions were predominant (74% of all Cx36-labeled gap junctions in the IPL). However, string plus ribbon gap junctions, previously reported only in the OPL, were found to be major subclasses of gap junctions in the IPL, accounting for nearly half (48%) of neuronal gap junctions in the OFF sublamina.

Based on striking differences between conventional plaque vs. string and ribbon gap junctions, as well as their first detection in IPL under photopic conditions, we tested the hypothesis that string gap junctions might reflect an extreme stage of light-adaptation-dependent or anesthesia-

dependent plasticity. Instead, we found that in the IPL of rats and mice prepared under photopic-, scotopic-and mesopic-adapted conditions, with and without general anesthesia, string and ribbon gap junctions remained abundant in the OFF sublamina and extremely rare in the ON sublamina. Thus, we found no evidence for differential light-adaptation-dependent or anesthesia-dependent structural rearrangement of plaques to form string gap junctions or of strings to be reconfigured as plaques. These results suggest that under constant illumination, string and ribbon gap junctions are normal components in the repertoire of gap junctions in the OFF sublamina of rats and mice.

Quantitative analysis of gap junctions: FRIL vs. LM

The number of connexons in neuronal gap junctions in mammalian retina ranges over four orders of magnitude [4 to 40,000 connexon pairs; ranges calculated from FRIL (rat and mouse; this report) and from TEM images of rabbit (Kolb, 1979; Strettoi et al., 1992)]. With this huge range of gap junction sizes, as well as the 2.3-fold higher volume-density of connexons in the ON vs. OFF sublaminae, confocal detection sensitivity must be reduced to avoid pixel saturation or image overlap of adjacent large puncta in the ON sublamina (Fig. 12A). This may have prevented visualization of very small (i.e. <50 connexons) gap junctions or diffusely stained gap junctions (i.e. string gap junctions; compare Fig. 12A vs. 12B). The same lower detection limit of fluorescence microscopy may also minimize simultaneous detection of two or more connexin proteins within small gap junctions (<100 connexons), where immunofluorescence for the less abundant connexin may not be detected, resulting in “false-negative” co-localization. Similar detection limits are also likely to occur when only a few fluorescent tracer molecules are able to permeate via very small gap junctions (Murphy et al., 1983).

Gap junctions in ON sublamina

In the ON sublamina of rabbit retina, 98% of the detected puncta were demonstrated to be on AII amacrine cells (Mills et al., 2001). By FRIL, ca. 95% of gap junctions in the ON sublamina were plaques. Notwithstanding possible species differences, these data taken together indicate that most gap junctions on AII amacrine cells in the ON sublamina correspond to plaques. Furthermore, 96% of the plaque gap junctions in the ON sublamina of photopic rat retina had crystalline configurations of their connexons (this report). Because AII amacrine cells in the ON sublamina are *minimally* electrically coupled under both dark-adapted and light-adapted conditions but maximally coupled under mesopic conditions (Bloomfield and Völgyi, 2004), most or all of the crystalline plaque gap junctions that we observed under photopic conditions must be minimally coupled. Conversely, our analysis of IPL in a limited number of retinas from mice prepared under mesopic conditions (Table 1) revealed an apparent fivefold increase in plaque gap junctions having connexons in non-crystalline configurations (preliminary observations). Both of these observations are consistent with suggestions that partial dispersal of connexons occurs coincident with an *increase* in coupling (Raviola et al., 1980). However, in fish retina, up to twofold dispersal of connexons occurred in plaque gap junctions of horizontal cells under different conditions of illumination, pH, and dopamine application associated with decreased gap junction coupling (Kurz-Isler and Wolburg, 1986; Wolburg and Rohlmann, 1995). The basis for these contradictory observations is not known.

Gap junctions are abundant in the OFF sublamina

By LM, Cx36-immunofluorescent puncta had been reported at much lower density in the OFF sublamina than in the ON sublamina (Feigenspan et al., 2001; Mills et al., 2001). In contrast, FRIL revealed equal volume-density of Cx36-containing gap junctions in both OFF and ON sublaminae; and by immunofluorescence, we found abundant but mostly small puncta at the limit of detectability, particularly in stratum 2. The abundant gap junctions in the OFF

sublaminae of rats and mice and the unusual linear configuration of half of these junctions constitute strong evidence for the existence of previously undescribed coupling pathways in the OFF sublamina of these two animal species with rod-dominant retinas.

Which neuron types have gap junctions in the OFF sublamina?

For scotopic and mesopic vision, rod pathways rely exclusively on and are superimposed ("piggybacked") on cone pathways (Kolb, 1979; Strettoi et al., 1992), which are abundant even in rod-dominant retinas. Rod bipolar cells synapse with AII amacrine cells in the ON-sublamina, with one pathway leading through ON-cone bipolar cells to ON-center ganglion cells, where Cx36 containing gap junctions have an essential role in linking AII amacrine to ON-cone bipolar cells (Deans et al., 2002). The same AII amacrine cells send abundant dendrites into the OFF sublamina, where they make chemical synapses with OFF-cone bipolar cells (Strettoi et al., 1992). Although gap junctions were not previously found on AII amacrine cells in the OFF sublamina (Strettoi et al., 1992), it is unlikely that string gap junctions, even though abundant, would have been detected by thin sectioning methods. Thus, our FRIL data indicating abundant Cx36-containing string gap junctions in the OFF sublamina open the possibility for a parallel rod OFF signaling pathway, from rod bipolar cells via chemical synapses to AII amacrine cells, thence via gap junctions to OFF cone-bipolar cells, and finally to OFF-center ganglion cells. (Also see Sharpe and Stockman, 1999; Völgyi et al., 2004.)

In addition to string and ribbon gap junctions, there are also abundant small (<100 connexons) and medium (100–400 connexon) plaque gap junctions in the OFF sublamina. Kolb (1979) suggested that many small gap junctions, presumably plaques, were between OFF cone bipolar axon terminals. In addition, electrical communication has been described between alpha ganglion cell dendrites in the OFF sublamina (Hu and Bloomfield, 2003; Hidaka et al., 2004; Schubert et al., 2005a). Many of the small plaque gap junctions observed by FRIL were between small processes that apparently had no synaptic vesicles, consistent with the possibility that they were between ganglion cells. However, without the ability to trace neurites to their cells of origin in FRIL replicas, and in the current absence of cell-specific labels for retinal neurons in FRIL, positive identification of either or both cells contributing to gap junctions was usually not possible.

Structural basis for diverse gap junction morphologies

Individual strands within string gap junctions were sometimes very long (ca. 130 connexons). However, other strands were discontinuous, containing 2 to 10 connexons per segment, with alignment of contiguous string segments across small gaps on either P- or E-faces, suggesting an underlying linear scaffolding structure (i.e. cytoplasmic filament) that ultrastructurally bridges successive segments (Fig. 14, model A). In addition, short "tethering" proteins may be required for establishing regular close packing, particularly in crystalline plaques (Fig. 14, model B). Although "self-affinity" of connexons could account for crystalline plaque formation, neither self-affinity, nor filaments, nor short tethers alone could account for formation of *non-crystalline* plaques, which have variable but larger spacings between adjacent connexons (Fig. 14, model C). Non-crystalline plaques would seem to require either a surrounding cytoplasmic "fence" (not illustrated), a change in tether length, or an additional class of somewhat longer tethers that would allow short-range dispersion of connexons. However, neither filaments nor tethers alone could produce ribbons, which may require both components to produce precise alignment of connexon doublets or triplets within these narrow bands of connexons (Fig. 14, model D).

Several cytoskeletal scaffolding and regulatory proteins at gap junctions have already been identified, including the PDZ domain-containing scaffolding proteins ZO-1 and ZO-2 and the signaling protein ZONAB (ZO-1-associated nucleic acid binding protein). Each of these has

been localized by confocal microscopy and FRIL at Cx36-containing gap junctions in adult rat retina (Li et al., 2004; Rash et al., 2004; Ciolofan et al., 2006). In addition, structural associations of connexins with actin and other PDZ-domain-containing scaffolding proteins (Giepmans and Moolenaar, 1998; Herve et al., 2004) may contribute to the hypothesized mechanisms for targeting and assembly of connexons into the several morphologies of gap junctions. The "filaments plus tethers" model is consistent with TEM studies of neuronal gap junctions in mammalian CNS, which describe "cytoplasmic semi-dense material" ca. 15 nm from gap junction contacts, as well as indistinct cross-bridges linking the cytoplasmic densities to the gap junctions (Sotelo and Korn, 1978; Kolb, 1979; Kosaka and Kosaka, 2005). This semi-dense cytoplasmic matrix presumably contains the proteinaceous scaffolding that labels for ZO-1, ZO-2 and ZONAB (Li et al., 2004; Rash et al., 2004; Ciolofan et al., 2006). This FRIL labeling also demonstrates that SDS does not wash away these apparently strongly-bound cytoplasmic proteins.

Possible physiological relevance of string and ribbon gap junctions

The physiological roles of string and ribbon gap junctions are unknown. However, we note that string gap junctions occupy 10–20 times the area of conventional plaque gap junctions having the same number of connexons (D_C=5:1–20:1). Thus, plaque gap junctions may provide for sub-cellular "pin-point" localization of intercellular signals (calcium ions, second messengers, etc.), whereas string gap junctions may provide a mechanism to disperse intercellular signals more widely within the synaptic contact area. Alternatively, linear arrays of connexons could represent either a unique morphology for functional intercellular channels or a morphology associated with non-functional channels that are, nevertheless, *structurally* coupled. A third possibility is that wide dispersion may set temporal constraints on re-assembly into more compact forms.

Although string and ribbon gap junctions provide the most recognizable feature of the IPL of rat and mouse retinas (both of which are rod-dominant), no data are currently available regarding the existence of string and ribbon gap junctions in the IPL of any other animal species, nor are there data available regarding possible unusual properties of electrical- or dye-coupling of neurons in the OFF sublamina of either of these two species. FRIL examination of retinas in other animal species is required to determine if similar configurations of connexons occur only in rod-dominant retinas (nocturnal rodents), cone-dominant retinas (e.g. diurnal ground squirrels), or in non-rodent species with cone-dominant foveas plus mixed rod/cone peripheral retinas, as in monkeys and humans. Likewise, FRIL analysis will be required to ascertain if gap junction morphologies are altered under rapidly-changing illumination conditions. Such comparative analysis will be essential for selecting appropriate models for examining the physiology of these unique gap junctions and their relevance to human vision.

Acknowledgements

Supported by NIH grants NS-44010, NS-44395 (J.E.R.), MH-062296 (G.E.P.) and the CIHR (J.I.N.). We thank Prof. Ray Whalen, DVM, for halothane anesthesiology and Brett Mclean for expert technical assistance. We also thank Dr. John O'Brien for helpful comments regarding the revised manuscript. Finally, we thank the journal reviewers for their very constructive criticisms and suggestions.

References

Bennett MVL. Gap junctions as electrical synapses. J Neurocytol 1997;26:349–366. [PubMed: 9278865]

Bloomfield SA, Völgyi B. Function and plasticity of homologous coupling between AII amacrine cells. Vision Res 2004;44:3297–3306. [PubMed: 15535997]

Branton D. Fracture faces of frozen membranes. Proc Natl Acad Sci U S A 1966;55:1048–1056. [PubMed: 5334198]

Ciolofan C, Li X, Olson C, Kamasawa N, Yasumura T, Morita M, Rash JE, Nagy JI. Association of connexin36 and ZO-1 with ZO-2 and the MsY3 transcription factor ZO-1 associated nucleic acid-binding protein (ZONAB) in mouse retina. Neuroscience 2006;140:433–451. [PubMed: 16650609]

Condorelli DF, Parenti R, Spinella F, Salinaro AT, Belluardo N, Cardile V, Cicirata F. Cloning of a new gap junction gene (Cx36) highly expressed in mammalian brain neurons. Eur J Neurosci 1998;10:1202–1208. [PubMed: 9753189]

Cook JE, Becker DL. Gap junctions in the vertebrate retina. Microsc Res Tech 1995;31:408–419. [PubMed: 8534902]

Deans MR, Völgyi B, Goodenough DA, Bloomfield SA, Paul DL. Connexin36 is essential for transmission of rod-mediated visual signals in the mammalian retina. Neuron 2002;36:703–712. [PubMed: 12441058]

Dinchuk JE, Johnson TJA, Rash JE. Postreplication labeling of E-leaflet molecules: Membrane immunoglobulins localized in sectioned labeled replicas examined by TEM and HVEM. J Electron Microsc Tech 1987;7:1–16. [PubMed: 2464678]

Dowling, JE. The retina. Cambridge: Belknap Press; 1987.

Dowling JE, Boycott BB. Organization of the primate retina: electron microscopy. Proc R Soc Lond B Biol Sci 1966;166:80–111. [PubMed: 4382694]

Euler T, Wässle H. Immunocytochemical identification of cone bipolar cells in the rat retina. J Comp Neurol 1995;361:461–478. [PubMed: 8550893]

Feigenspan A, Janssen-Bienhold U, Hormuzdi S, Monyer H, Degen J, Söhl G, Willecke K, Ammermuller J, Weiler R. Expression of connexin36 in cone pedicles and OFF-cone bipolar cells of the mouse retina. J Neurosci 2004;24:3325–3334. [PubMed: 15056712]

Feigenspan A, Teubner B, Willecke K, Weiler R. Expression of neuronal connexin36 in AII amacrine cells of the mammalian retina. J Neurosci 2001;21:230–239. [PubMed: 11150340]

Fujimoto K. Freeze-fracture replica electron microscopy combined with SDS digestion for cytochemical labeling of integral membrane proteins. Application to the immunogold labeling of intercellular junctional complexes. J Cell Sci 1995;108:3443–3449. [PubMed: 8586656]

Giepmans BN, Moolenaar WH. The gap junction protein connexin43 interacts with the second PDZ domain of the zonula occludens-1 protein. Curr Biol 1998;8:931–934. [PubMed: 9707407]

Güldenagel M, Söhl G, Plum A, Traub O, Teubner B, Weiler R, Willecke K. Expression patterns of connexin genes in mouse retina. J Comp Neurol 2000;425:193–201. [PubMed: 10954839]

Han Y, Massey SC. Electrical synapses in retinal ON cone bipolar cells: Subtype-specific expression of connexins. Proc Natl Acad Sci U S A 2005;102:13313–13318. [PubMed: 16150718]

Herve JC, Bourmeyster N, Sarrouilhe D. Diversity in protein-protein interactions of connexins: emerging roles. Biochim Biophys Acta 2004;1662:22–41. [PubMed: 15033577]

Heuser JE, Reese TS, Dennis MJ, Jan Y, Jan L, Evans L. Synaptic vesicle exocytosis captured by quick freezing and correlated with quantal transmitter release. J Cell Biol 1981;275:275–300.

Hidaka S, Akahori Y, Kurosawa Y. Dendrodendritic electrical synapses between mammalian retinal ganglion cells. J Neurosci 2004;24:10553–10567. [PubMed: 15548670]

Hidaka S, Kato T, Miyachi E. Expression of gap junction connexin36 in adult rat retinal ganglion cells. J Integr Neurosci 2002;1:3–22. [PubMed: 15011262]

Hirokawa N, Heuser J. The inside and outside of gap-junction membranes visualized by deep etching. Cell 1982;30:395–406. [PubMed: 6814761]

Hombach S, Janssen-Bienhold U, Söhl G, Schubert T, Bussow H, Ott T, Weiler R, Willecke K. Functional expression of connexin57 in horizontal cells of the mouse retina. Eur J Neurosci 2004;19:2633–2640. [PubMed: 15147297]

Hu EH, Bloomfield SA. Gap junctional coupling underlies the short-latency spike synchrony of retinal α ganglion cells. J Neurosci 2003;23:6768–6777. [PubMed: 12890770]

Kolb H. The inner plexiform layer in the retina of the cat: electron microscopic observations. J Neurocytol 1979;8:295–329. [PubMed: 490185]

Kolb H, Famiglietti EV. Rod and cone pathways in the inner plexiform layer of cat retina. Science 1974;186:47–49. [PubMed: 4417736]

Kosaka T, Kosaka K. Intraglomerular dendritic link connected by gap junctions and chemical synapses in the mouse main olfactory bulb: Electron microscopic serial section analyses. Neuroscience 2005;131:611–625. [PubMed: 15730867]

Kurz-Isler G, Wolburg H. Gap junctions between horizontal cells in the cyprinid fish alter rapidly their structure during light and dark adaptation. Neurol Lett 1986;67:7–12.

LaVail MM. Survival of some photoreceptor cells in albino rats following long-term exposure to continuous light. Invest Opthal 1976;15:64–70.

Li X, Olson C, Lu S, Kamasawa N, Yasumura T, Rash JE, Nagy JI. Neuronal connexin36 association with zonula occludens-1 protein (ZO-1) in mouse brain and interaction with the first PDZ domain of ZO-1. Eur J Neurosci 2004;19:2132–2146. [PubMed: 15090040]

Matsubara A, Laake JH, Davanger S, Usami S, Ottersen OP. Organization of AMPA receptor subunits at a glutamate synapse: A quantitative immunogold analysis of hair cell synapses in the rat organ of Corti. J Neurosci 1996;16:4457–4467. [PubMed: 8699256]

Maul, GG. Temperature-dependent changes in intramembrane particle distribution. In: Rash, JE.; Hudson, CS., editors. Freeze fracture: methods, artifacts and interpretations. New York: Raven Press; 1979. p. 37-42.

Maxeiner S, Dedek K, Janssen-Bienhold U, Ammermuller J, Brune H, Kirsch T, Pieper M, Degen J, Kruger O, Willecke K, Weiler R. Deletion of connexin45 in mouse retinal neurons disrupts the rod/cone signaling pathway between AII amacrine and ON cone bipolar cells and leads to impaired visual transmission. J Neuroscience 2005;25:566–576.

Maxeiner S, Kruger O, Schilling K, Traub O, Urschel S, Willecke K. Spatiotemporal transcription of connexin45 during brain development results in neuronal expression in adult mice. Neuroscience 2003;119:689–700. [PubMed: 12809690]

Meier C, Dermietzel R, Davidson KGV, Yasumura T, Rash JE. Connexin32-containing gap junctions in Schwann cells at the internodal zone of partial myelin compaction and in Schmidt-Lanterman incisures. J Neurosci 2004;24:3186–3198. [PubMed: 15056698]

Mills SL, O'Brien JJ, Li W, O'Brien J, Massey SC. Rod pathways in the mammalian retina use connexin 36. J Comp Neurol 2001;436:336–350. [PubMed: 11438934]

Murphy AD, Hadley RD, Kater SB. Axotomy-induced parallel increases in electrical and dye coupling between identified neurons of Helisoma. J Neurosci 1983;3:1422–1429. [PubMed: 6306177]

Nagy JI, Patel D, Ochalski PAY, Stelmack GL. Connexin30 in rodent, cat and human brain: Selective expression in gray matter astrocytes, co-localization with connexin43 at gap junctions and late developmental appearance. Neuroscience 1999;88:447–468. [PubMed: 10197766]

Nelson R. Cat cones have rod input: a comparison of the response properties of cones and horizontal cell bodies in the retina of the cat. J Comp Neurol 1977;172:109–135. [PubMed: 838876]

Ottersen OP, Landsend AS. Organization of glutamate receptors at the synapse. Eur J Neurosci 1997;9:2219–2224. [PubMed: 9464917]

Pereda A, O'Brien J, Nagy JI, Bukauskas F, Davidson KGV, Kamasawa N, Yasumura T, Rash JE. Connexin35 mediates electrical transmission at mixed synapses on Mauthner cells. J Neurosci 2003a; 23:7489–7503. [PubMed: 12930787]

Pereda A, O'Brien J, Nagy JI, Smith M, Bukauskas F, Davidson KGV, Kamasawa N, Yasumura T, Rash JE. Short-range functional interaction between connexin35 and neighboring chemical synapses. Cell Commun Adhes 2003b;10:419–423. [PubMed: 14681051]

Pereda A, Rash JE, Nagy JI, Bennett MVL. Dynamics of electrical transmission at club endings on the Mauthner cells. Brain Res Brain Res Rev 2004;47:227–244. [PubMed: 15572174]

Rash, JE.; Dillman, R.; Morita, M.; Whalen, LR.; Guthrie, PB.; Fay-Guthrie, D.; Wheeler, DW. Grid-mapped freeze fracture: correlative confocal laser scanning microscopy and freeze-fracture electron microscopy of preselected neurons in spinal cord slices. In: Shotton, DM.; Severs, NJ., editors. Techniques in modern biomedical microscopy. 2. New York: Wiley-Liss; 1995. p. 127-150.Rapid freezing, freeze-fracture and deep etching

Rash JE, Duffy HS, Dudek FE, Bilhartz BL, Whalen LR, Yasumura T. Grid-mapped freeze-fracture analysis of gap junctions in gray and white matter of adult rat central nervous system, with evidence for a "panglial syncytium" that is not coupled to neurons. J Comp Neurol 1997;388:265–292. [PubMed: 9368841]

Rash JE, Pereda A, Kamasawa N, Furman CS, Yasumura T, Davidson KGV, Dudek FE, Olson C, Nagy JI. High-resolution proteomic mapping in the vertebrate central nervous system: Close proximity of connexin35 to NMDA glutamate receptor clusters and co-localization of connexin36 with immunoreactivity for zonula occludens protein-1 (ZO-1). J Neurocytol 2004;33:131–152. [PubMed: 15173637]

Rash JE, Staines WA, Yasumura T, Patel D, Hudson CS, Stelmack GL, Nagy JI. Immunogold evidence that neuronal gap junctions in adult rat brain and spinal cord contain connexin36 (Cx36) but not Cx32 or Cx43. Proc Natl Acad Sci U S A 2000;97:7573–7578. [PubMed: 10861019]

Rash JE, Yasumura T. Improved structural detail in freeze-fracture replicas: High-angle shadowing of gap junctions cooled below −170° C and protected by liquid nitrogen-cooled shrouds. J Electron Microsc Tech 1992;20:187–204.

Rash JE, Yasumura T. Direct immunogold labeling of connexins and aquaporin4 in freeze-fracture replicas of liver, brain and spinal cord: factors limiting quantitative analysis. Cell Tissue Res 1999;296:307–321. [PubMed: 10382274]

Rash JE, Yasumura T, Dudek FE, Nagy JI. Cell-specific expression of connexins, and evidence for restricted gap junctional coupling between glial cells and between neurons. J Neurosci 2001;21:1983–2001. [PubMed: 11245683]

Raviola E, Gilula NB. Gap junctions between photoreceptor cells in the vertebrate retina. Proc Natl Acad Sci U S A 1973;70:1677–1681. [PubMed: 4198274]

Raviola E, Gilula NB. Intramembrane organization of specialized contacts in the outer plexiform layer of the retina. J Cell Biol 1975;65:192–222. [PubMed: 1127010]

Raviola E, Goodenough DA, Raviola G. Structure of rapidly frozen gap junctions. J Cell Biol 1980;87:273–279. [PubMed: 7419595]

Raviola E, Raviola G. Structure of the synaptic membranes in the inner plexiform layer of the retina: a freeze-fracture study in monkeys and rabbits. J Comp Neurol 1982;209:233–248. [PubMed: 7130454]

Reale E, Luciano L, Spitznas M. Communicating junctions of the human sensory retina. Albrecht Von Graefes Arch Klin Exp Ophthalmol 1978;208:77–92. [PubMed: 310266]

Schubert T, Degen J, Willecke K, Hormuzdi S, Monyer H, Weiler R. Connexin36 mediates gap junctional coupling of alpha-ganglion cells in mouse retina. J Comp Neurol 2005a;485:191–201. [PubMed: 15791644]

Schubert T, Maxeiner S, Kruger O, Willecke K, Weiler R. Connexin45 mediates gap junctional coupling of bistratified ganglion cells in the mouse retina. J Comp Neurol 2005b;490:29 –39. [PubMed: 16041717]

Sharpe T, Stockman A. Rod pathways: the importance of seeing nothing. Trends Neurosci 1999;22:497–504. [PubMed: 10529817]

Sotelo C, Korn H. Morphological correlates of electrical and other interactions through low-resistance pathways between neurons of the vertebrate central nervous system. Int Rev Cytol 1978;55:67–107. [PubMed: 389866]

Staehelin LA. Structure and function of intercellular junctions. Int Rev Cytol 1974;39:191–283. [PubMed: 4611943]

Steere RL, Erbe EF, Moseley JM. Prefracture and cold-fracture images of yeast plasma membranes. J Cell Biol 1980;86:113–122. [PubMed: 6998983]

Sterling, P.; Demb, JB. Retina. In: Shepherd, GM., editor. The synaptic organization of the brain. New York: Oxford; 2004. p. 217-269.

Strettoi E, Raviola E, Dacheux RF. Synaptic connections of the narrow-field, bistratified rod amacrine cell (AII) in the rabbit retina. J Comp Neurol 1992;325:152–168. [PubMed: 1460111]

Tsukamoto Y, Morigiwa K, Ueda M, Sterling P. Microcircuits for night vision in mouse retina. J Neurosci 2001;21:8616–8623. [PubMed: 11606649]

Vaney DI. Retinal neurons: cell types and coupled networks. Prog Brain Res 2002;136:239–254. [PubMed: 12143385]

Völgyi B, Deans MR, Paul DL, Bloomfield SA. Convergence and segregation of the multiple rod pathways in mammalian retina. J Neurosci 2004;24:11182–11192. [PubMed: 15590935]

Wässle H. Parallel processing in the mammalian retina. Nat Rev Neurosci 2004;5:747–757. [PubMed: 15378035]

Wolburg H, Rohlmann A. Structure-function relationships in gap junctions. Int Rev Cytol 1995;157:315–373. [PubMed: 7706021]

Abbreviations

Cx36
connexin36

Cx45
connexin45

Cx57
connexin57

D_C
dispersion coefficient

E-face
extraplasmic fracture face

FRIL
freeze-fracture replica immunogold labeling

GCL
ganglion cell layer

IgG
immunoglobulin G

IMP
intramembrane particle (also, intramembrane protein)

INL
inner nuclear layer

IPL
inner plexiform layer

LE
labeling efficiency

LM
light microscopy

ONL
outer nuclear layer

OPL
outer plexiform layer

P-face
protoplasmic fracture face

PSD
postsynaptic density

SDS

sodium dodecylsulfate detergent

SPB

Sørensen's phosphate buffer

TBSTr

Tris buffered saline plus 0.3% Triton X-100

TEM

transmission electron microscopy

ZO-1

zonula occludens-1

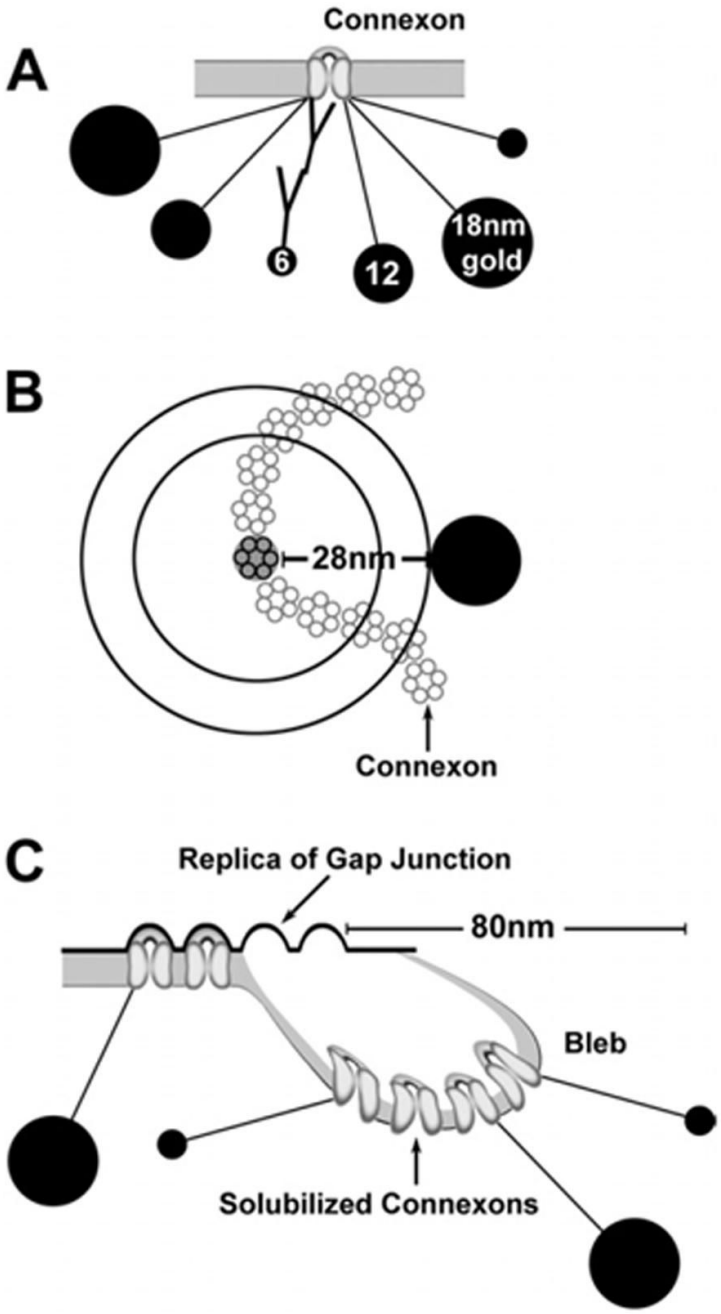

Fig. 1.

Scale drawing of immunogold-labeled connexons and gap junctions. (A) Relative sizes of immunogold beads (6-nm, 12-nm and 18-nm) and 28-nm length of double-antibody bridges hemispherically linking gold beads to one connexon. (B) Immunogold labeling of one connexon within a string gap junction. Without air drying, 100% of labels fall at or within the outer circle, with 50% falling within the inner circle, whose radius is one-half the $\sqrt{2}$ multiplied by the 28-nm radius of uncertainty (i.e. 0.707 × 28 nm = 21 nm). With air drying, most if not all gold beads dry radially to the outer circle. (C) Incompletely solubilized lipid bleb, as immobilized by air drying before it could detach and be released into the SDS solution. In TEM

images of blebs, labels for displaced connexons may be 50–80 nm from the margin of replicated gap junctions (Rash and Yasumura, 1999).

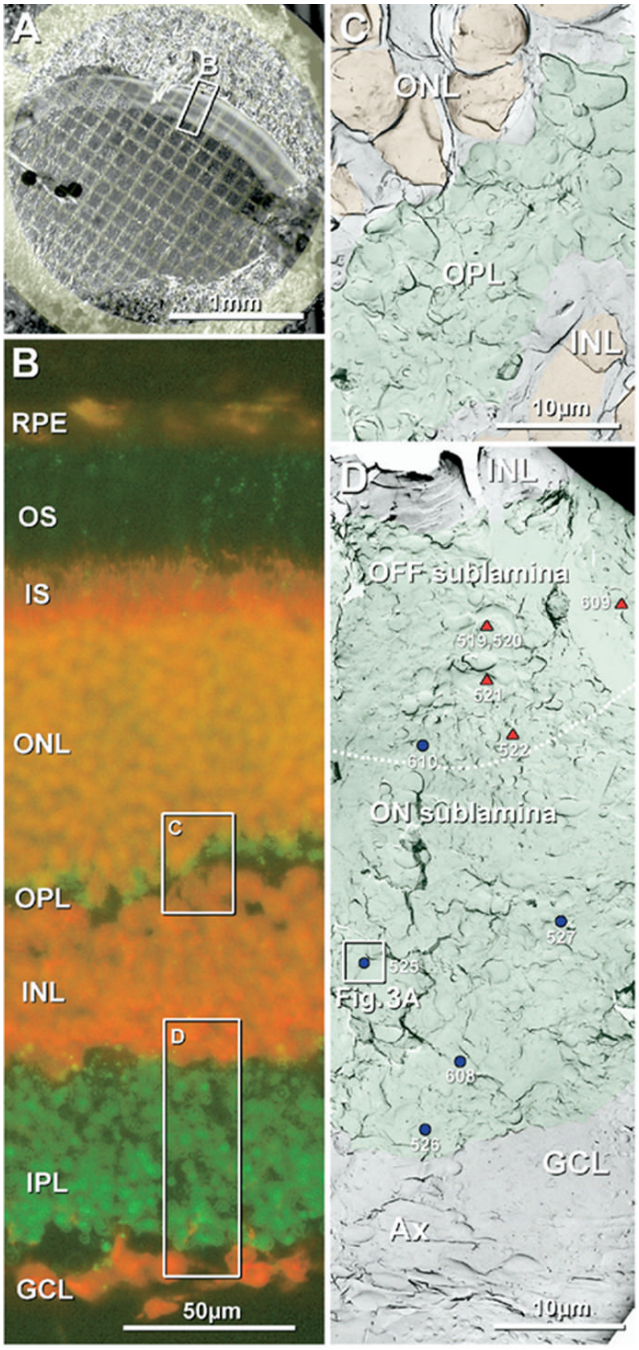

Fig. 2.

Confocal light microscopic and FRIL images of rat retina used for photomapping. (A) Confocal image of freeze-fractured retina bonded in Lexan on a gold “index” grid. Tissue autofluorescence revealed three cytoplasmic layers: OS and IS (outer bright band), as well as the neuropil-rich OPL (middle thin band) and IPL (broad inner bright band). (B) Confocal image showing Cx36 immunofluorescence (green) and fluorescent Nissl staining (red). Cx36-positive puncta form a thin, almost discontinuous layer in OPL (green fluorescence; upper box, C) and a much thicker layer in IPL (wider green fluorescence, lower box, D). Nuclei in the ONL, INL, and GCL are bright red. Inscribed areas C, D have corresponding FRIL images as Fig. 1C, D. RPE, retinal pigment epithelium, OS, outer segment of photoreceptor cells; IS,

inner segment of photoreceptor cells. (C) Low magnification FRIL image of the OPL (green overlays), which forms a thin layer of neuropil between the ONL and the INL. Nuclei of the ONL and INL (orange overlay) were identified by nuclear pores in double nuclear membranes and by cross-fractures through the nucleoplasm. (D) Low magnification FRIL image of the IPL (green overlay) between the INL and GCL. Triangles and dots correspond to positions of gap junctions, each identified by a number assigned according to the order in which it was found. Red triangles, individual string gap junctions; blue dots, plaque gap junctions. The dotted white line indicates the approximate border between OFF and ON sublaminae, approximately 2/5 distance from the edge of the INL and 3/5 from the GCL. Boxed area contains a gap junction that is shown at high magnification as Fig. 3A. Scale bars are as indicated in each panel.

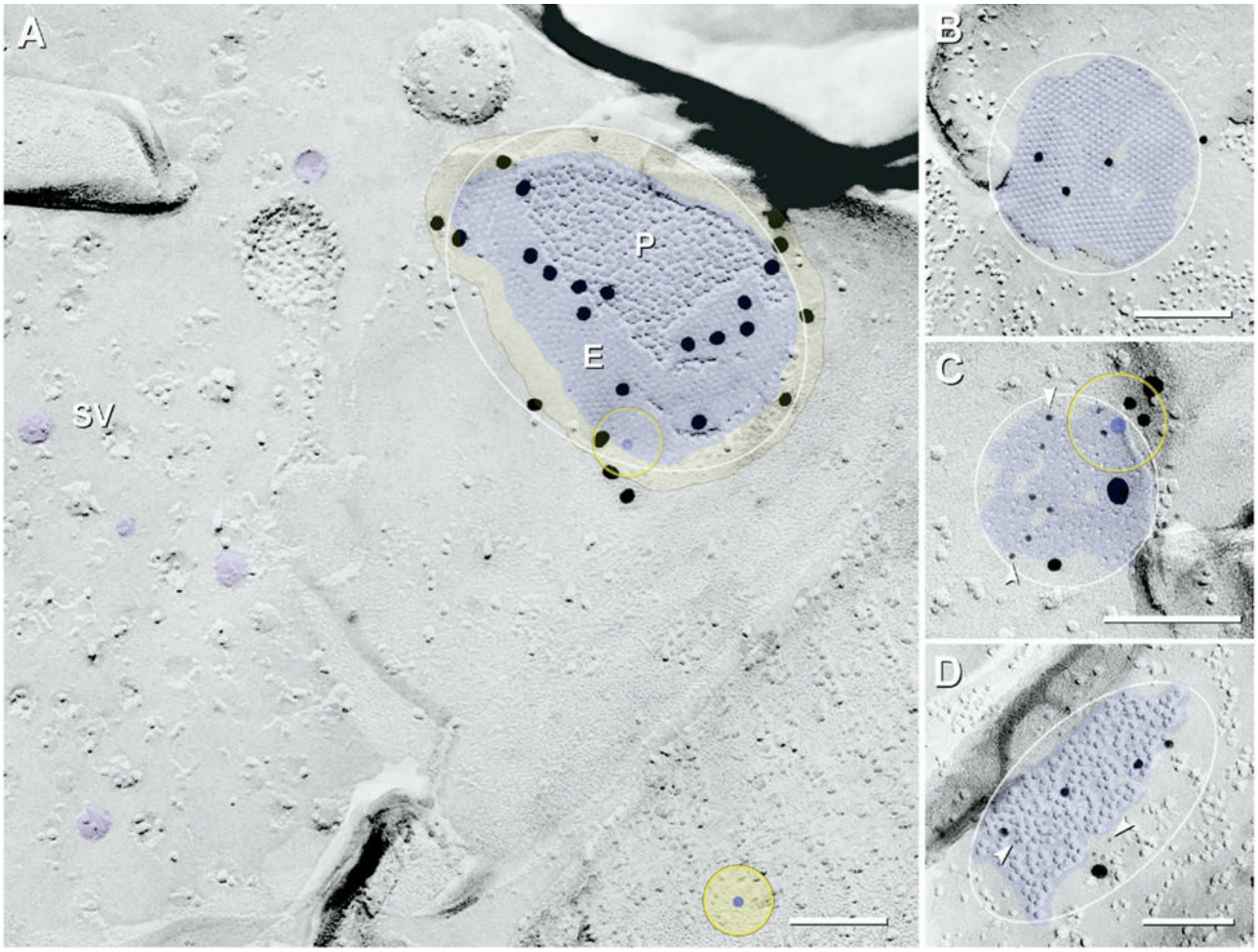

Fig. 3.

FRIL images of "crystalline" and "non-crystalline" plaque gap junctions (blue overlay) labeled for Cx36. (A) Large crystalline plaque (ca. 900 connexons labeled by 24 18-nm gold beads) linking E-face of post-synaptic membrane to P-face of pre-synaptic membrane in the ON sublamina. Synaptic terminal contains densely packed synaptic vesicles (SV, purple overlays). Note absence of non-specific background labeling and absence of labeling >50 nm outside of the gap junction. The E-face (E) of the gap junction is labeled at substantially higher density than its P-face (P). Inscribed ellipses were used to calculate D_C for the different configurations of gap junctions. Yellow overlay with outline, zone of immunogold labeling for connexons at edge of gap junction. Yellow target with blue center, circle of potential labeling, as applied to a single hypothetical connexon, superimposed as a circle with 33 nm radius centered around a 9-nm connexon (28 nm+4.5 nm; see Experimental Procedures). (B) E-face image of large crystalline plaque gap junction having clearly delineated "domains" of quasi-crystalline hexagonal E-face pits (ca. 570 connexons; four 10-nm gold beads; low LE). Small voids (areas of no color) exist at intersections of domains. (C) E-face image of small-diameter non-crystalline plaque gap junction in ON sublamina [ca. 90 connexons, labeled by 10 6-nm gold beads, arrowheads, and two 18-nm gold beads (both for polyclonal Cx36 antibody) and by three 12-nm gold beads (for monoclonal Cx36 antibody)]. (D) P-face image of medium-diameter non-crystalline plaque gap junction in ON sublamina [ca. 200 connexons; labeled by 10 6-nm gold beads, arrowheads, and one 18-nm gold bead (for polyclonal Cx36 antibody) and by four 12-nm gold beads (for monoclonal Cx36 antibody)]. Scale bars=0.1 μm.

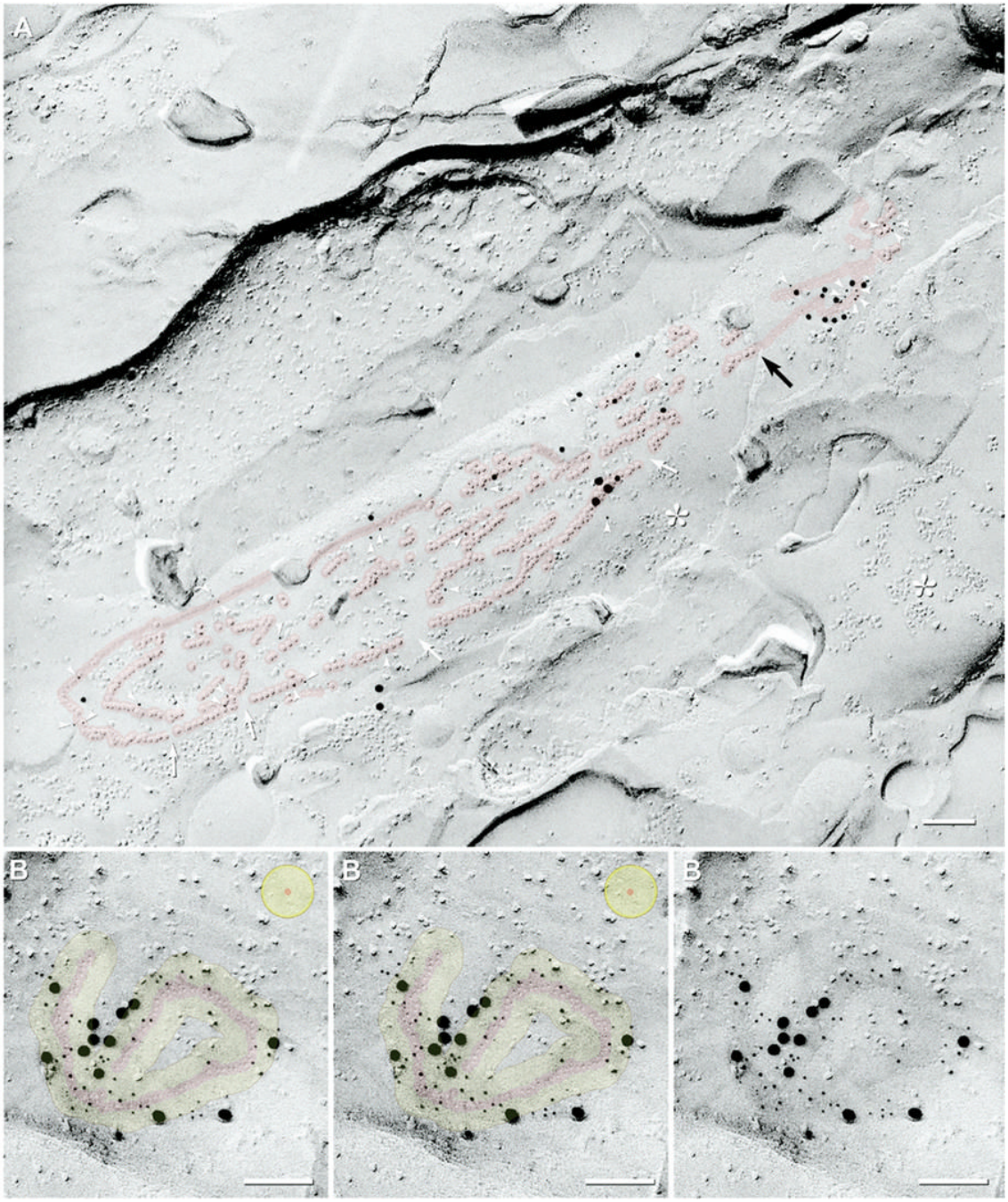

Fig. 4.

FRIL images of "string" gap junctions labeled for Cx36. (A) P-face image of a large multi-stranded string gap junction (ca. 520 connexons; ca. 0.3 μm×2 μm, red overlay) in the proximal half of the OFF sublamina (stratum 2); double-labeled for Cx36 and ZO-1 (31 6-nm gold beads, arrowheads; and 18 12-nm plus gold beads for Cx36; five 18-nm gold beads for ZO-1). Rows of P-face connexon IMPs and E-face connexon imprints are 0.02–0.7 μm long and contain two to 70 connexons each. Successive segments are well aligned, but small discontinuities are evident (white arrows). Several strings have short segments that are two connexons wide. The extracellular space is narrowed to 3 nm where the connexon strand steps between P- and E-face (black arrow). * Unidentified IMPs, distinguished from connexons by their variable sizes

(4–12 nm) and irregular spacing. (B) Stereoscopic (left pair) and reverse stereoscopic (right pair) E-face image of a convoluted single-strand string gap junction (ca. 120 connexons, red overlay) in the OFF sublamina; labeled by 54 6-nm and 12 18-nm gold beads (for polyclonal Cx36 antibody) and by one 12-nm gold bead (for monoclonal Cx36 antibody). Yellow overlay, zone of immunogold labeling for a target connexon. Approximately 90–95% of gold beads are within the red and yellow overlays. Some minor clumping of gold beads is evident. Yellow target (top right), circle of potential labeling for one hypothetical connexon. Scale bars=0.1 μm.

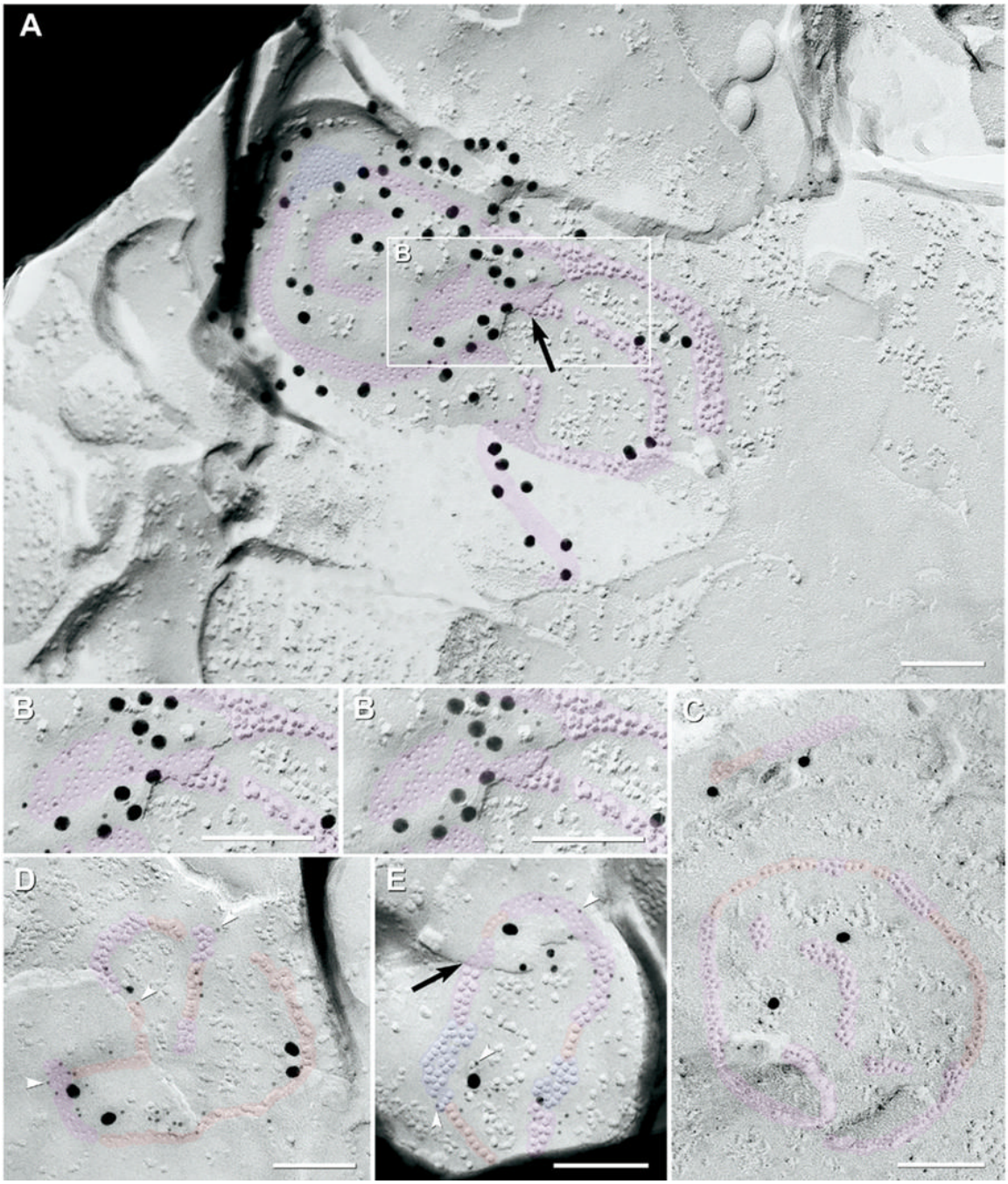

Fig. 5.

FRIL images of "ribbon" gap junctions labeled for Cx36. (A) Large multi-strand ribbon gap junction (ca. 490 connexons; pink overlay, plus small blue overlay for plaque-like portion) in the proximal half of the OFF sublamina (stratum 2); sequentially double-labeled for Cx36 by ca. 40 6-nm gold beads (for the first polyclonal anti-Cx36 antibody) and 52 18-nm gold beads (for the second polyclonal anti-Cx36 antibody). P-face IMPs and E-face pits are in ribbons that are two and three connexons wide. Notably, E-face connexon pits (which are above unfractured connexons of the lower cell) were labeled at a density about 10 times greater than the P-face IMPs. Black arrow, narrowed extracellular space at the point the fracture-plane stepped from P- to E-face. Due to local angle of shadow, a portion of the gap junction not shadowed by

platinum (pink “tail” at bottom) was identified in stereoscopic views of the original TEM negatives (not shown). (B) High magnification reverse stereoscopic image of inscribed area of (A). Note the abundant 6-nm gold beads on the E-face of the gap junction (left side). (C) Medium-size (ca. 220 connexons) composite ribbon gap junction (pink overlay) containing a substantial portion as strings (red overlay). Labeled by four 18-nm gold beads. (D) Medium-size gap junction (ca. 150 connexons) consisting of string and ribbon configurations (red and pink segments); designated as string gap junction based on its majority component. The gap junction is labeled by 28 6-nm (arrowheads) and four 18-nm gold beads (for polyclonal Cx36 antibody) and by one 12-nm gold bead (for monoclonal Cx36 antibody). (E) Medium-diameter gap junction (ca. 130 connexons) consisting of ribbon (pink), string (red) and plaque-like portions (blue overlay). Labeled by 19 6-nm (arrowheads) and two 18-nm gold beads (for polyclonal Cx36 antibody) and by four 12-nm gold beads (for monoclonal Cx36 antibody). Black arrow, narrowed extracellular space at the point the fracture-plane stepped from P- to E-face within the gap junction. Scale bars=0.1 μm.

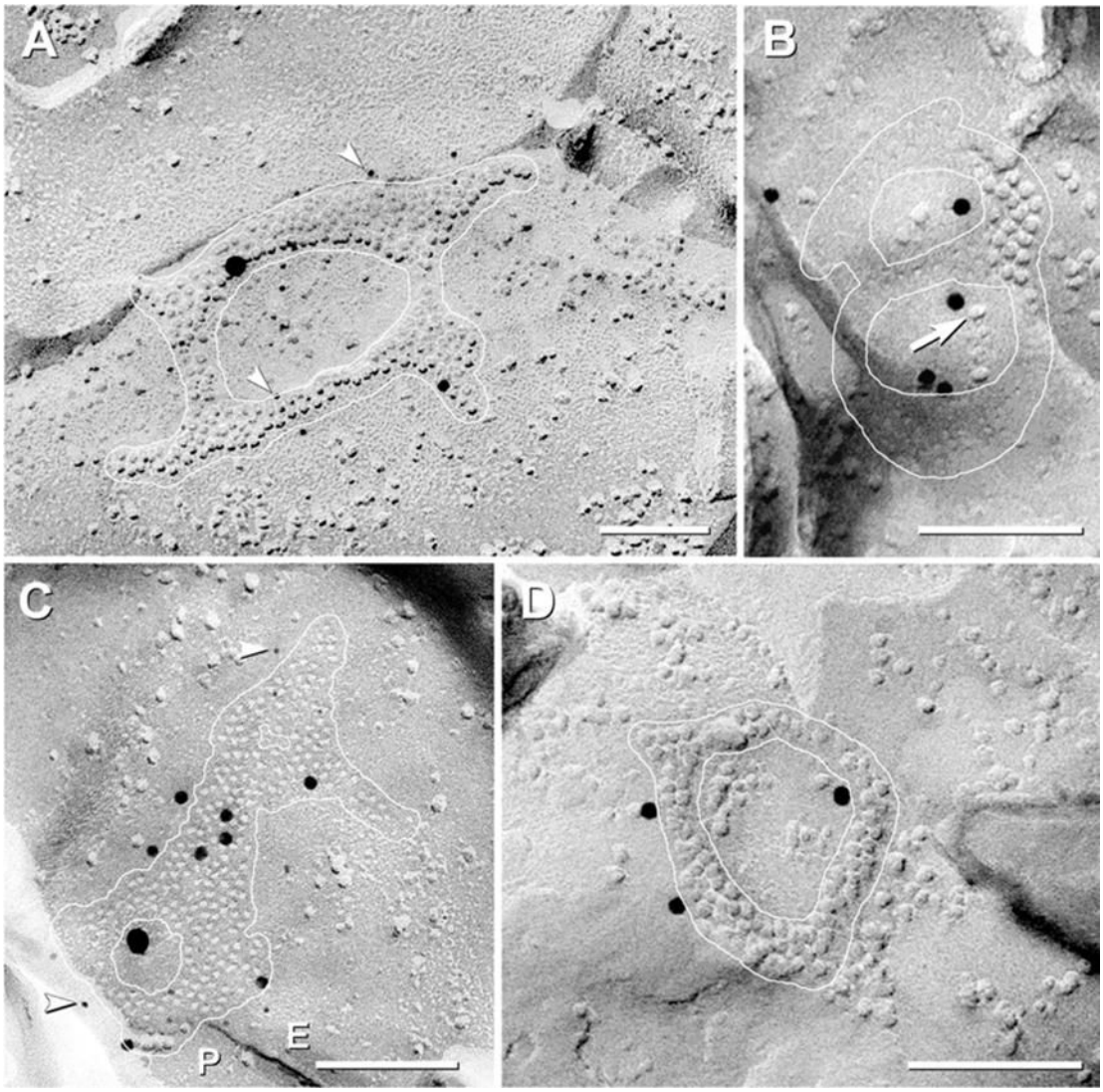

Fig. 6.

FRIL images of rat and mouse "reticular" gap junctions (white outline) labeled for Cx36. (A) Reticular gap junction in ON sublamina. Connexon-free voids are large enough to contain >100 connexons. The ca. 230 P-face connexons are double-labeled for Cx36 by 14 6-nm gold beads (arrowheads) and one 18-nm gold bead (for polyclonal Cx36 antibody) and by one 12-nm gold bead (for monoclonal Cx36 antibody). (B) Medium reticular gap junction in ON sublamina; ca. 120 connexons forming the numeral "8" are single-labeled for Cx36 by ca. five 12-nm gold beads. E-face particles (arrow) occur within voids. (Low contrast due to vertical shadowing.) (C) Medium reticular gap junction in OFF sublamina; ca. 220 connexon E-face pits are double-labeled for Cx36 by nine 6-nm gold beads (arrowheads) and one 18-nm gold bead (for monoclonal antibody) plus seven 12-nm gold beads (for polyclonal antibody). Two small connexon-free voids are present within the gap junction. (D) Small reticular gap junction in mouse OFF sublamina. Approximately 94 connexons are labeled for Cx36 by three 12-nm gold beads. Scale bars=0.1 μm.

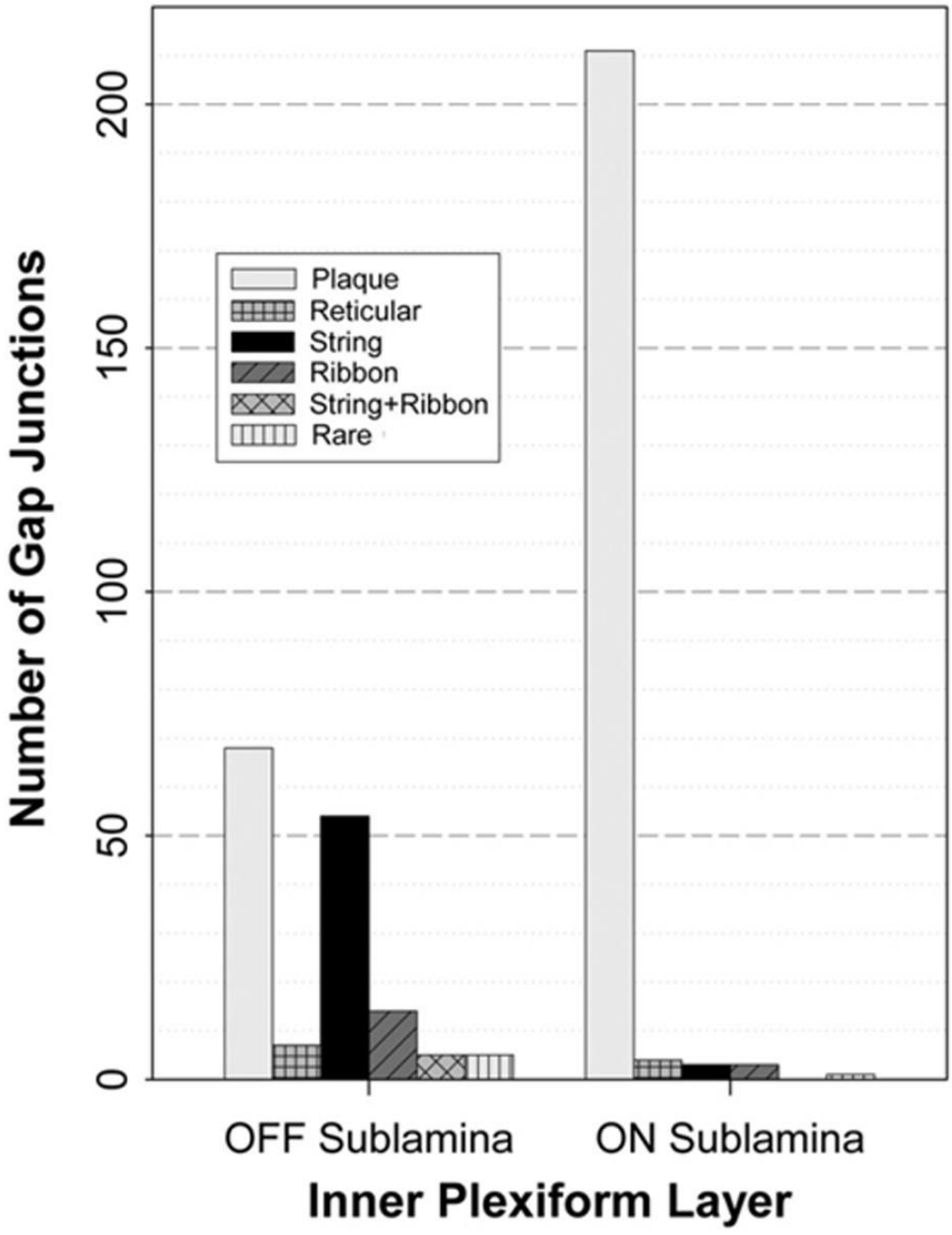

Fig. 7.

Histogram showing numbers of each of five distinctive configurations of gap junctions in ON vs. OFF sublamina of light-adapted rat retina. Bars indicate the numbers of gap junctions. Of all mapped gap junctions, 40.8% (153/375) were in the OFF sublamina and 59.2% (222/375) were in the ON sublamina, corresponding closely to the 2:3 thickness ratio of OFF vs. ON sublaminae, thereby demonstrating equivalent volume density of gap junctions in both sublaminae. However, plaque gap junctions (light gray bars) were more concentrated in the ON sublamina, reticular gap junctions (bars with horizontal cross-hatch) were rare but were found in both sublaminae, and string gap junctions (black bars) and ribbon gap junctions (bars with diagonal lines) were restricted almost exclusively to the OFF sublamina. Bar with diagonal

cross-hatch represents rarer intermixed configurations of string and ribbon gap junctions, as found only in the OFF sublamina. Bars with vertical lines indicate rare configurations of gap junctions.

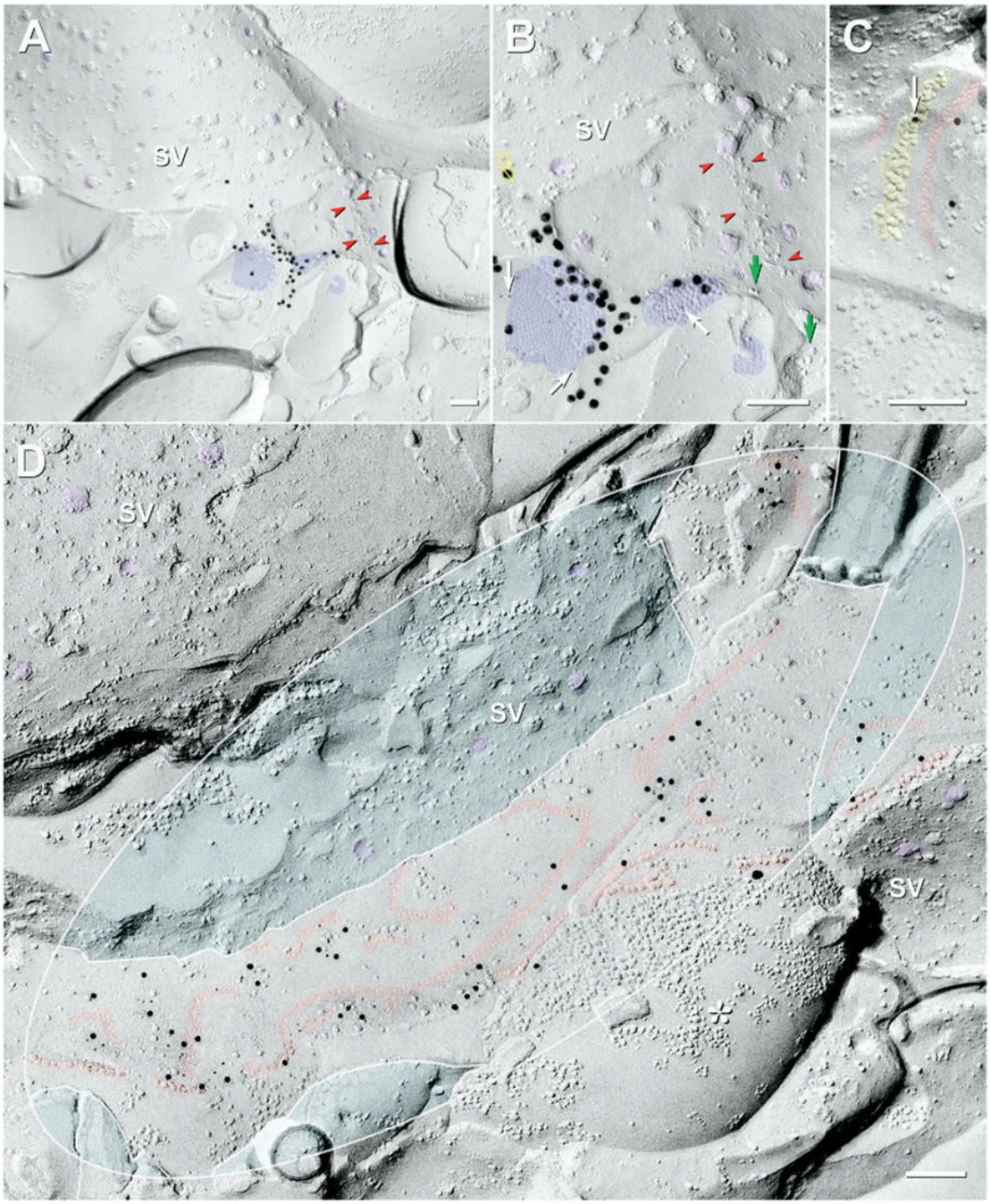

Fig. 8.

Mixed (A–C) and "functionally-mixed" (D) synapses in ON and OFF sublaminae. (A) Large-diameter synapse in ON sublamina. Distinctive presynaptic ribbon is characteristic of bipolar cell terminals. Synaptic vesicles (SV, purple overlays) crowd against the presynaptic ribbon (red arrowheads). Two of three gap junctions (blue overlays) are within 0.1 μm of the synaptic ribbon. (B) At higher magnification, the larger two gap junctions are crystalline plaques, both of which are well labeled for Cx36, and the third (ca. 16 connexons) is irregular and unlabeled. The larger gap junction is labeled for Cx36 by nine 6-nm (white arrows) and ca. 34 18-nm gold beads. Due to the stochastic nature of immunogold labeling, absence of gold on the smallest gap junction does not necessarily indicate absence of Cx36. Green arrows, IMPs of presumptive

active zones; Yellow circles with bars, non-specific gold beads on the top surface of the replica (determined by viewing stereo pairs). (C) Two small string gap junctions (red overlays) parallel to postsynaptic density characteristic of ribbon synapses (yellow overlay). One of three gold beads (arrow) for Cx36 is partially obscured by the PSD, but is nevertheless, within the zone of immunogold labeling for both string gap junctions. (D) E-face image of compound string gap junction at "functionally mixed" synapse (Pereda et al., 2003b, 2004) on large synaptic expansion in OFF sublamina. Its ca. 320 connexons (mostly E-face pits) are double-labeled for Cx36 and ZO-1 (45 12-nm gold beads and 80 6-nm gold beads for Cx36; one 18-nm gold bead for ZO-1; possible labeling). SV (purple overlays) are in the cytoplasms of two of the cells linked by gap junction strands. The gap junction includes an 80 connexon-long strand (0.8 μm long) and several shorter strands (up to 40 connexons long). Some strands end with small plaque-like clusters of connexons. In one nerve terminal P-face (asterisk, lower right), unidentified non-connexon IMPs of various diameters are tightly clumped due to phase separation during formaldehyde fixation, whereas connexons are of uniform diameter and are separated by uniform 10-nm center-to-center spacing. Inscribed ellipse was used to calculate D_C. The turquoise areas were subtracted from the areas used for calculating D_C because the fracture plane entered the cytoplasm (upper left) and because, in the second case, a separate gap junction strand was linked to a different axon terminal, also identified by its content of SV (right). D_C=21.1. Scale bars=0.1 μm.

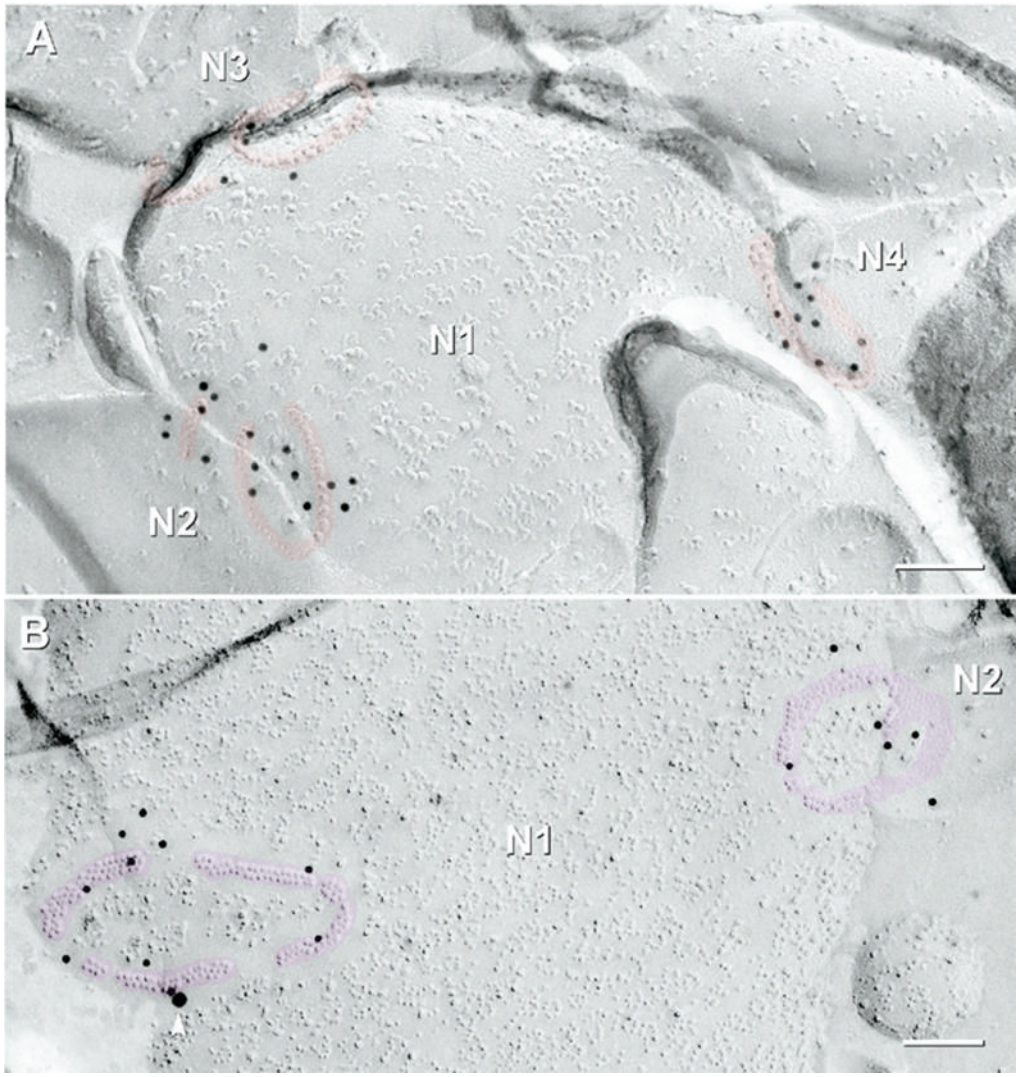

Fig. 9.

Multiple string (red overlays) and ribbon gap junctions (pink overlays), labeled for Cx36, link one neurite to multiple neurites. (A) Three string gap junctions labeled for Cx36 by 12-nm gold beads on one neurite P-face (N1) linking to three different neurites (N2–N4) in the OFF sublamina. A small compound gap junction (an incomplete circle and an adjacent strand, ca. 40 connexons) formed one synaptic contact between neurite N1 and neurite N2. Two small circular string gap junctions (ca. 40 connexons) linking N1 to N3 have both string and ribbon portions. A small tilted circular gap junction (ca. 30 connexons) links N1 to N4. (B) Two medium-diameter ribbon gap junctions in the P-face of an unmapped neurite (N1) were labeled for Cx36. The left gap junction (ca. 165 connexons) consisted of four segments of crystalline ribbon; labeled by 10 12-nm gold beads. The right gap junction (N1 to N2) contains mixed ribbon and reticular portions (ca. 220 connexons labeled by six 12-nm gold beads). The single 18-nm gold bead (arrowhead) is confirmed as rare nonspecific labeling because it is on the Lexan-coated non-tissue side of the replica (stereoscopic images not shown). Scale bars=0.1 μm.

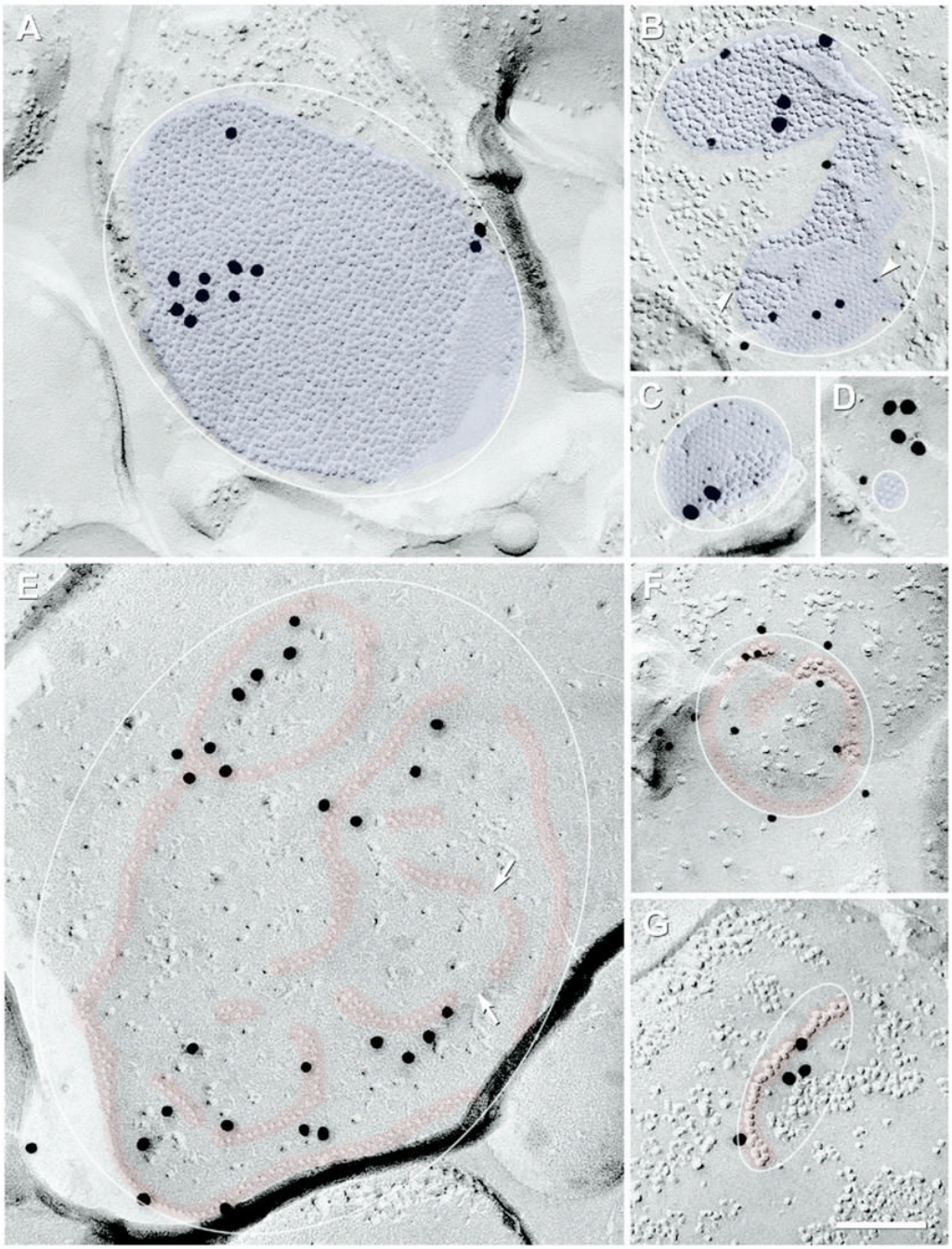

Fig. 10.

FRIL images of large-, medium-, and small-diameter plaque (blue overlays) and string (red overlays) gap junctions, all at the same magnification. Inscribed ellipses were used to calculate D_C for the different configurations of gap junctions; details in Experimental Procedures. (A) The largest plaque gap junction found under baseline photopic conditions consisted of ca. 1800 connexons labeled by 11 18-nm gold beads (0.35×0.5 μm; unmapped). (This FRIL replica had low LE.) (B) Large irregularly-shaped crystalline gap junction in OFF sublamina (ca. 550 connexons) double-labeled for Cx36 by seven 6-nm gold beads (arrowheads) and seven 12-nm gold beads, and for ZO-1 by three 18-nm gold beads. (C) Medium-diameter crystalline plaque gap junction in ON sublamina; ca. 180 IMPs are labeled for Cx36 by 12 6-nm and two

18-nm gold beads. Plaque with smooth margin on one side and truncated margin on the opposite side contained the nearly maximum density of connexons (12,000 connexons/μm^2, D_C=1.0). (D) Tiny crystalline plaque gap junction in OFF sublamina. Its 11 E-face pits are labeled for Cx36 by one 12-nm gold bead and four (possibly clumped) 18-nm gold beads (see Experimental Procedures for criteria used to designate specificity of labeling). (E) Compound string gap junction (ca. 240 connexon pits) single-labeled for Cx36 by 26 20-nm gold beads (unmapped). Despite its fivefold larger diameter, it contains only slightly more connexons than the gap junction in (C). Discontinuities occur between strands of connexons (arrows). (F) Small circular string gap junction with ca. 65 connexons labeled for Cx36 by 12 12-nm gold beads (OFF sublamina). (G) Single-strand string gap junction in the OFF sublamina of IPL [similar to one in OPL described by Raviola and Gilula (1973)]; labeled for Cx36 by four 18-nm gold beads on 32 connexon IMPs. Scale bar=0.1 μm.

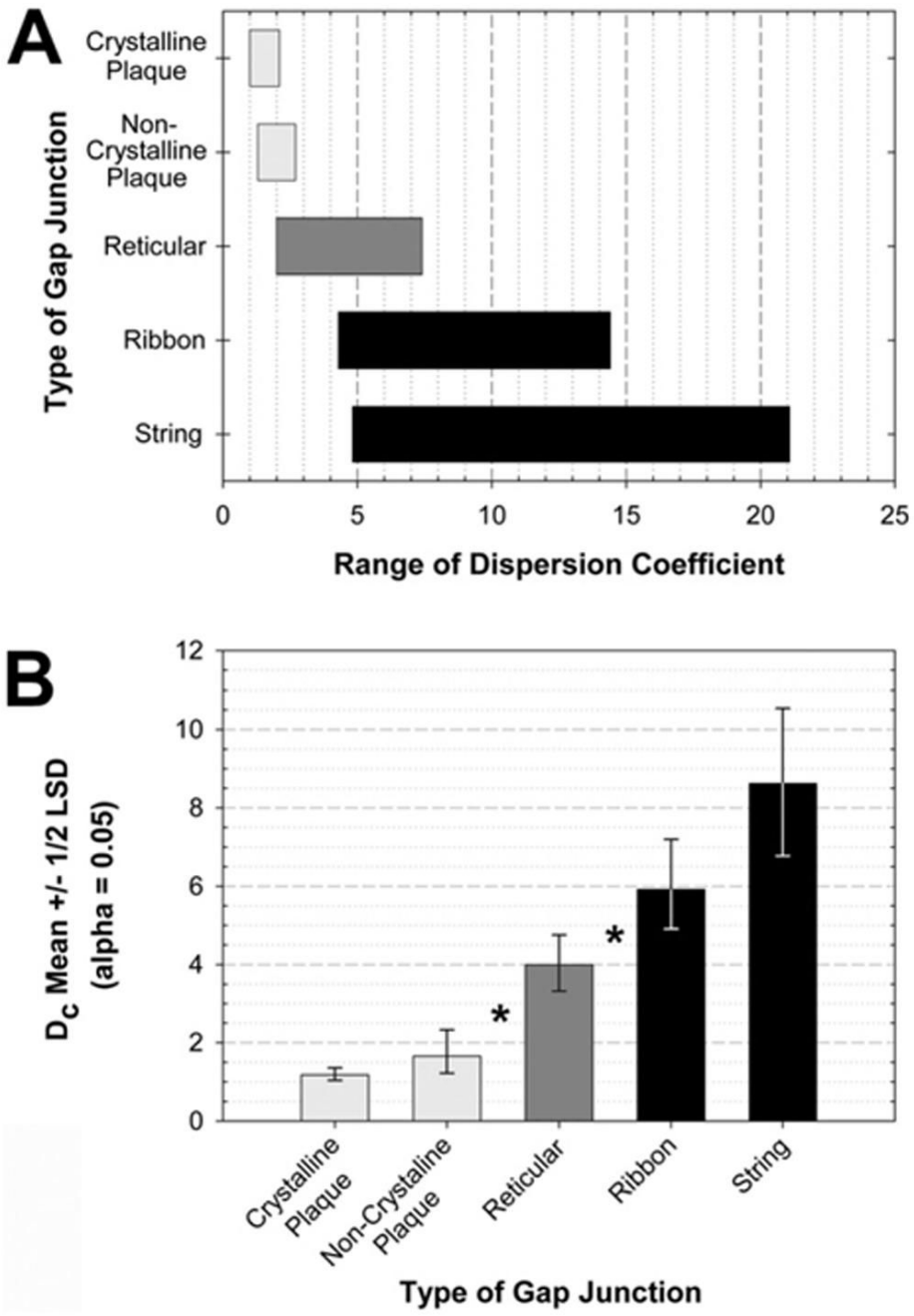

Fig. 11.

Range of D_C for the five primary configurations of gap junctions. (A) Range of D_C for each configuration of gap junction. Bars indicate the range of dispersion of each type of array. (B) Statistical analysis for D_C. Means with ±1/2 least significant difference intervals, alpha=0.05. Means with intervals that do not overlap are significantly different, * $P<0.05$.

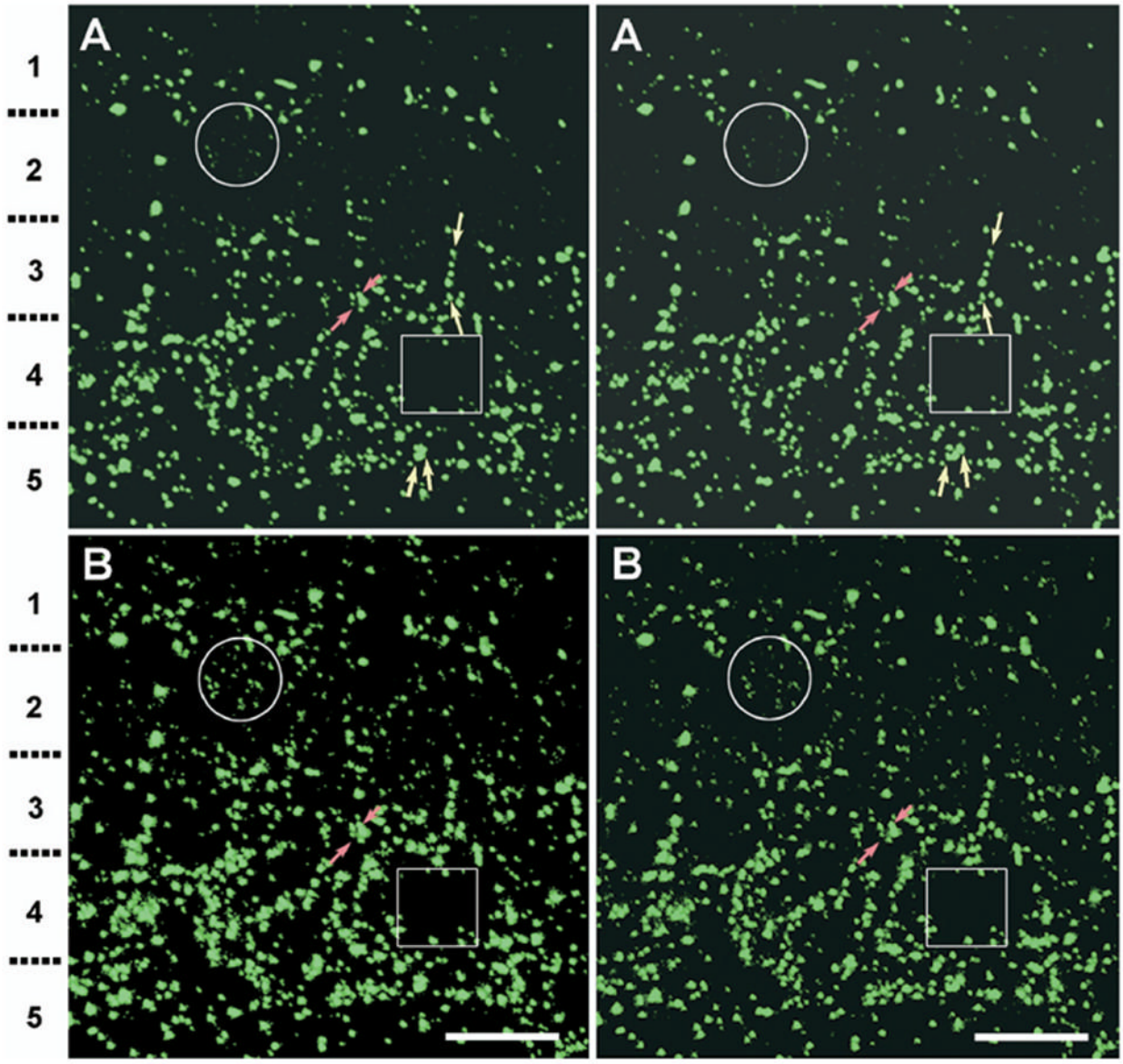

Fig. 12.

Stereoscopic confocal immunofluorescence images of Cx36-labeled puncta in adult rat IPL; shown at appropriate image contrast for visualization of large puncta (A), as well as following contrast expansion in the "dark output" range using "levels," with the "mid-range output" set close to the "low output" level, allowing visualization of small faint puncta (B). (A) Full thickness image of the IPL from its distal to proximal margins (top to bottom). Strata 1–5 are indicated on the left. Stereoscopic imaging reveals large to fine puncta in all strata and allows discrimination of adjacent or overlapping puncta seen in the Z-stack projection, and separately reveals puncta linearly arranged along the *z* axis (yellow arrows). The largest puncta are 0.8–1.5 μm in the longest dimension. (B) The same stereoscopic image, but with expanded contrast in the dark output range. Large numbers of additional, lightly-fluorescent puncta appear in the lower pair [compare circles in (A) vs. (B)]. Stratum 2 contains small puncta that are as abundant as the intense puncta in the ON sublamina (strata 3–5). In the ON sublamina, the same image intensification reveals few additional puncta [compare boxes in (A) vs. (B)]. Some puncta in (A) appear fused in (B) because of pixel halation (red arrows). Scale bar=10 μm.

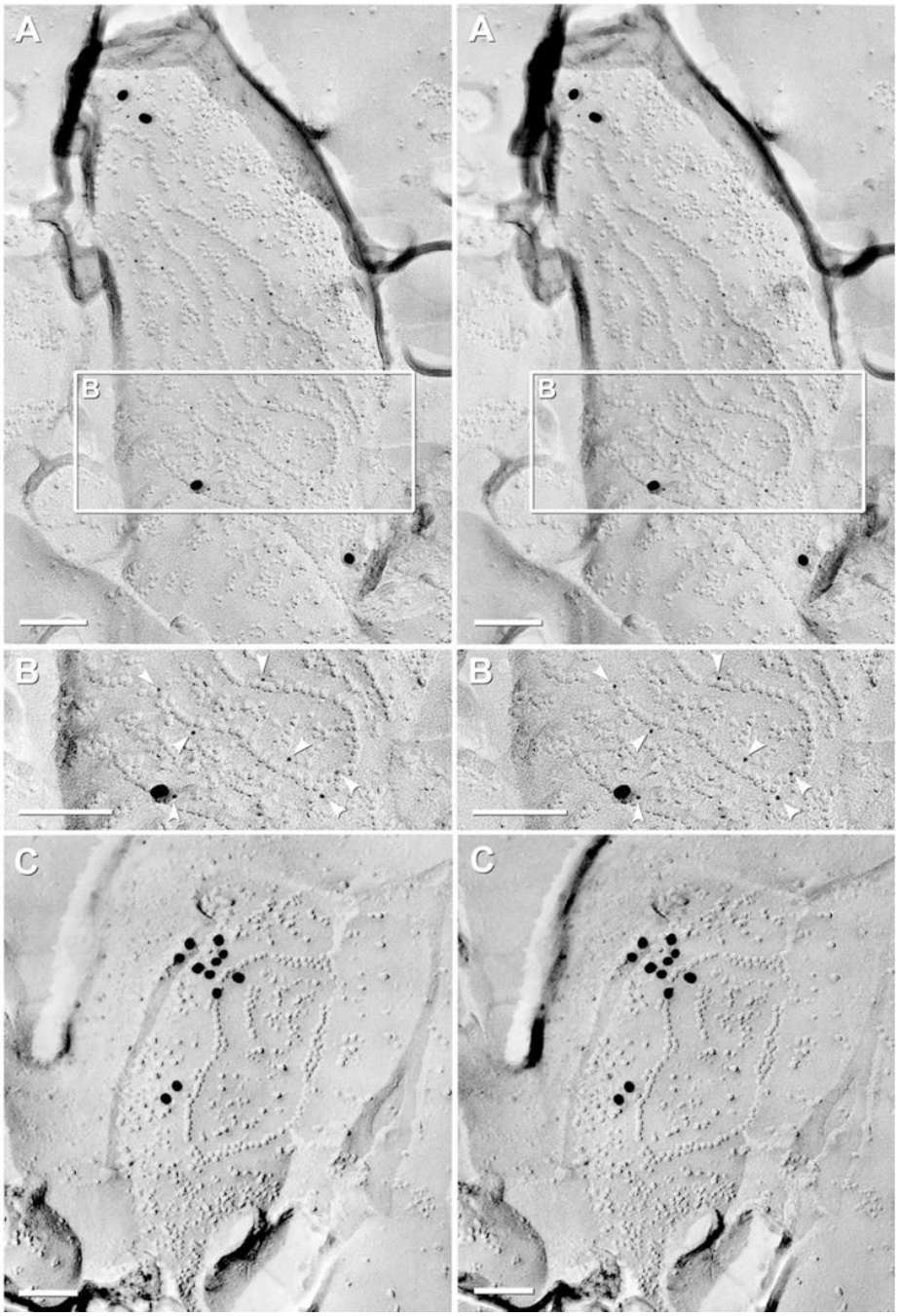

Fig. 13.

FRIL image of string gap junctions labeled for Cx36 in the OFF sublamina of rat and mouse retina. (A) Medium-sized string gap junction in rat fixed under *scotopic illumination without anesthesia*; labeled by four 18-nm plus 21 6-nm gold beads. (B) Reverse-stereoscopic image of the inscribed area in (A). The strands of connexons were particularly well labeled with 6-nm gold beads (arrowheads). (C) Small string gap junction in mouse retina fixed under *photopic illumination without anesthesia*; labeled by two small clumps of 18-nm gold beads. Scale bars=0.1 μm.

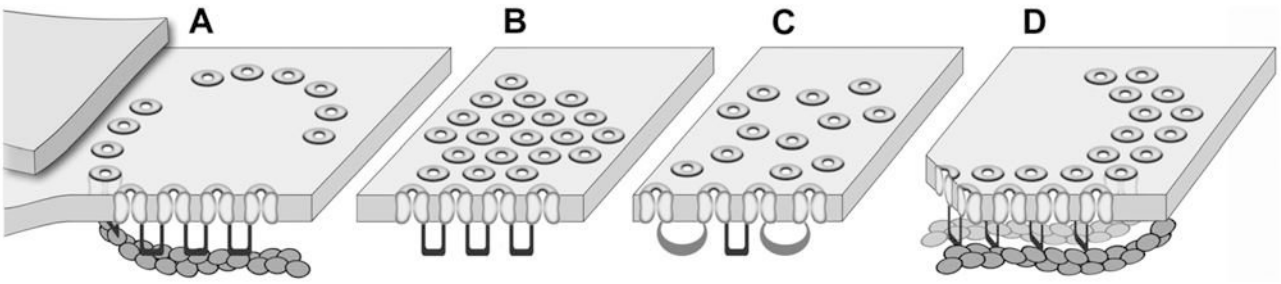

Fig. 14.

Diagram of hypothetical cytoplasmic filaments and tethers proposed to provide for morphological diversity of gap junctions. Cytoplasmic filaments are drawn as 6-nm filaments. (A) Connexons organized into strings by cytoplasmic filaments plus cross-bridges. (B) Connexons held in hexagonal close packing by short tethers. (C) Connexons held in non-crystalline arrays by short and long tethers. (D) Connexons held in ribbons by one to three cytoplasmic filaments plus short cross-bridges.

Table 1

Number of gap junctions detected under different conditions of illumination and under different conditions of anesthesia

	Photopic	Mesopic	Scotopic
Rats			
Anesthesia	649 (72[ab])	—	7[b]
CD	77	—	126
Mice			
Anesthesia[c]	158	96	181
CD	325	106	—

General anesthetics included ketamine/xylazine, halothane, and sodium pentobarbital. CD, cervical dislocation for killing.

[a] Ketamine/xylazine; used for statistical analysis.

[b] Barbital; not included in statistical analysis.

[c] Barbital or halothane.

Table 2

Number, types and laminar distributions of neuronal gap junctions (GJs) in the IPL of adult rat retina

Type of gap junction	Mapped GJs									Unmapped GJs sublamina undetermined				
	OFF sublamina				ON sublamina									
	S	M	L	$\sum_{OFF}$	S	M	L	$\sum_{ON}$	$\sum_{M}$	S	M	L	$\sum_{Un}$	$\sum_{T}$
Crystalline plaque	50	10	1	61	87	76	38	201	262	88	76	32	196	458
Non-crystalline plaque	6	0	0	6	7	2	1	10	16	5	0	0	5	21
Reticular	5	2	0	7	3	1	0	4	11	1	1	0	2	13
Ribbon	7	5	2	14	3	0	0	3	17	19	11	0	30	47
String	42	12	1	55	3	0	0	3	58	24	11	0	35	93
String+ribbon	3	2	0	5	0	0	0	0	5	0	3	0	3	8
Rare forms	4	0	1	5	1	0	0	1	6	2	1	0	3	9
Totals	117	31	5	153	104	79	39	222	375	139	103	32	274	649

L, large (>400 connexons); M, medium (100–400 connexons); S, small gap junctions (2–100 connexons); $\sum M$, sum of mapped gap junctions; $\sum OFF$, sum in OFF sublamina; $\sum ON$, sum in ON sublamina; $\sum T$, total each type in all locations; $\sum Un$, sum of unmapped gap junctions.